Protection of a 400 kV Parallel Overhead Line System with Series Compensation

Protection in the Transmission Network

Master's Thesis
Rasmus Laustsen

AALBORG UNIVERSITY

STUDENT REPORT

Title:
Protection of Parallel Cables in a Network with Weak Infeed Characteristics

Theme:
Electric Power Systems and High Voltage Engineering

Project Period:
Master thesis

Project Group:
EPSH4-1038

Participant(s):
Rasmus Laustsen

Supervisor(s):
Claus Leth Bak

Page Numbers: 70

Date of Completion:
May 27, 2025

Abstract:

This thesis investigates the performance of Energinet's standard protection system, comprising differential and distance relays, in detecting and isolating faults in a meshed transmission network with an integrated air-core reactor in series. The theoretical framework has indicated that the differential protection does not encounter difficulties when the air-core reactor is integrated. However, the distance relay encounters problems with the impedance settings, which can be attributed to the mutual coupling in the parallel line system and the added impedance from the air-core reactor. This thesis proposes a solution of having two sets of impedance settings for the distance relay that adapt based on the operational state of the air-core reactor. The solution has been tested through a series of PSCAD simulations. The results show that for single-line-to-ground faults, the relay overestimates the fault distance by 8 % to 13 %, while it provides accurate results for phase-to-phase and three-phase faults. The overestimation of the single-line to ground can be attributed to PSCAD's inaccuracy in accounting for the zero-sequence and mutual coupling. The simulated voltage and current waveforms for single-line-to-ground faults are used to calculate a theoretical fault location, achieving an accuracy within 1 % of the actual fault distance.

Preface

This master's thesis is made by the group EPSH4-1038 in the 4rd semester MSc of Energy at Aalborg University. The report is a master's thesis of the MSc studies with a specialization in Electrical Power Systems and High Voltage Engineering. The master's thesis is made between February 1st and May 28th, 2025. Group EPSH4-1038 wants to thank Supervisor Claus Leth Bak for excellent supervision.
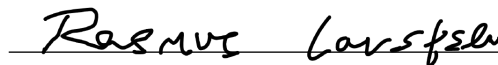
Reading Guide
This Master's thesis consists of eight chapters and three appendixes. Figures, tables, equations, and listings are numbered by the chapter or appendix, i.e. figures, tables, and listings have the same format, such as: Figure 1.1. Equations have a format with parentheses, such as: Equation (2.1).

Citations in this master's thesis use the IEEE citation format. The IEEE citation format starts with the citation number, author, title, type, and publication information. The reference list is sorted by the order of appearance in the report, such that the first citation in the report is the first citation in the reference list.

The following programs have been used during this master's thesis:

- Overleaf by WriteLatex Ltd
- InkScape by The InkScape Team
- PSCAD simulation tool
- Matlab by Mathworks

Aalborg University, May 27, 2025

Rasmus Laustsen
<rlaust20@student.aau.dk>

iv

Summery

Energinet aims to improve power flow control in the transmission system by adding an air-core reactor in series with the Endrup to Revsing 400 kV transmission line. Series air-core reactors control power flow by introducing a controllable line reactance into the transmission line, thereby increasing network impedance. However, the series air-core reactors provide challenges for a differential and a distance relay. This thesis will therefore investigate the performance of Energinet's standard protection system in detecting and isolating faults in a meshed transmission network with an integrated air-core reactor in series.

The theoretical framework shows that the differential protection does not encounter difficulties when the air-core reactor is integrated, assuming that the current transformer provides accurate measurements. However, the distance relay encounters problems as the line impedance is affected by the mutual coupling in the parallel line connection from Endrup to Revsing and the added impedance from the air-core reactor. This thesis proposes a solution of having two sets of impedance settings, which depend on the state of the series air-core reactor.

To verify the proposed solution, a PSCAD model is developed. The PSCAD model consists of the Endrup to Revsing connection, which includes the in-feed in Endrup and the upstream network from Revsing limited to two substations. The Endrup substation connects the COBRA *High Voltage Direct Current* (HVDC) link between Denmark and the Netherlands, as well as the offshore wind farms Horns Rev B and Horns Rev C, to the transmission network. Therefore, the in-feed at Endrup is considered to exhibit weak characteristics. In PSCAD, the in-feed at Endrup is modeled using reference models for offshore wind farms and HVDC systems to reflect the actual short-circuit contributions. Furthermore, is a remote source located at the end of the upstream network connected.

This means that during fault events in PSCAD, current contributions from both ends in-feeds will impact the fault characteristics and the calculated distance to the fault. This impact has been analyzed in PSCAD, where the simulation results have shown that a fault impedance lower than $1\,\Omega$ does not impact the distance to the fault. However, fault resistances of $5\,\Omega$ and above impact the accuracy of the distance to the fault significantly. The assessment of the distance relay has been conducted with a fault impedance of $0.01\,\Omega$; therefore, is the accuracy of the distance relay in compiling the distance to the fault not impacted by the current contributions from both ends.

The results obtained through PSCAD simulations regarding the assessment of the proposed solution for the distance relay have shown that for single-line-to-ground faults, the relay overestimates the fault distance by 8 % to 13 %, while it provides accurate results for phase-to-phase and three-phase faults. The overestimation of the single-line to ground can be attributed to PSCAD's inaccuracy in accounting for the zero-sequence and mutual coupling. The simulated voltage and current waveforms for single-line-to-ground faults are used to calculate a theoretical fault location, achieving an accuracy within 1 % of the actual fault distance. The method utilized to compile the theoretical distance to the fault is similar to the method that the Siemens 7SA522 distance relay from the SIPROTEC 4 series uses. Therefore, the solution of having two impedance settings for the distance relay is considered validated, within the scope of this master's thesis.

Nomenclature

Abbreviations

AC	Alternating Current
CB	Circuit Breaker
CT	Current Transformer
DFIG	Doubly-Fed Induction Generator
DSO	Distribution System Operator
DUTT	Direct Underreaching Transfer Trip
EMI	Electromagnetic Interference
EMT	Electromagnetic Transients
FCL	Fault Current Limiter
IBR	Inverter Based Renewables
IBR	Inverter-Based Resources
IGBT	Insulated-Gate Bipolar Transistor
LCC	Line-Commutated Converter
OHL	Overhead Line
PST	Phase-Shifting Transformer
PUTT	Permissive Overreaching Transfer Trip
PUTT	Permissive Underreaching Transfer Trip
PWM	Pulse Width Modulation
RES	Renewable Energy Sources
RMS	Root Mean Square
TSO	Transmission System Operator
VSC	Voltage Source Converter
VT	Voltage Transformer
WT	Wind Turbine

Symbols

α	Phase shifting angle	$^\circ$
δ	Phase angle difference between busbars	$^\circ$
κ	Short-circuit current factor	-
φ	Phase angle	$^\circ$
f	Frequency	Hz
I	Current	A
K	Constant	-
K_{0M}	Zero-sequence mutual compensation factor	-
K_0	Zero-sequence compensation factor	-
K_1	Steepness of slope	-
K_2	Steepness of slope	-
P	Active power	W
R	Resistance	Ω
V	Voltage	V
X	Reactance	L
Z	Impedance	Ω
t	Time	s

Physical constants

μ	Permability	d
ρ	Resistivity	Ωm
c	Speed of light	m/s

Contents

Chapter 1 Introduction

The Danish government has established climate goals with emission targets for reducing greenhouse gas emissions by 2030 and 2050. By 2030, Denmark aims to reduce emissions by 70 % compared to emissions from 1990 and by 2050 achieve net-zero emissions [1]. To accelerate the expansion of *Renewable Energy Sources* (RES) in the Danish grid, the climate agreement on green power and heat of June 2022 specifies that a minimum of 9 GW offshore wind energy must be constructed before the end of 2030 [2]. In addition, a continuous effort to harness solar energy is necessary to cover net electricity consumption [3].

The energy geographically would be placed in locations with high wind potential as the Danish East and West coast or in rural regions with ample space for *Photovoltaic* (PV) plants [2]. Consequently, moving energy production further away from the majority of energy demand in larger cities. This necessitates grid expansion as transmitting the energy over longer distances will add further stress to the electrical grid.

The growing stress on the transmission network is driving significant grid development efforts from Energinet, the *Transmission System Operator* (TSO) in Denmark. A notable example of this is the proposed solution to enhance power flow control in the transmission network by installing a series reactor or *Phase-Shifting Transformer* (PST) in the *Overhead Line* (OHL) connection from Endrup to Revsing. [4]

1.1   Transmission Network: Endrup-Revsing Connection

Energinet aims to improve power flow control within the transmission network, necessitating the implementation of either a series reactor or a PST. Figure 1.1 shows a section of the DK1 network with the series reactor implemented.
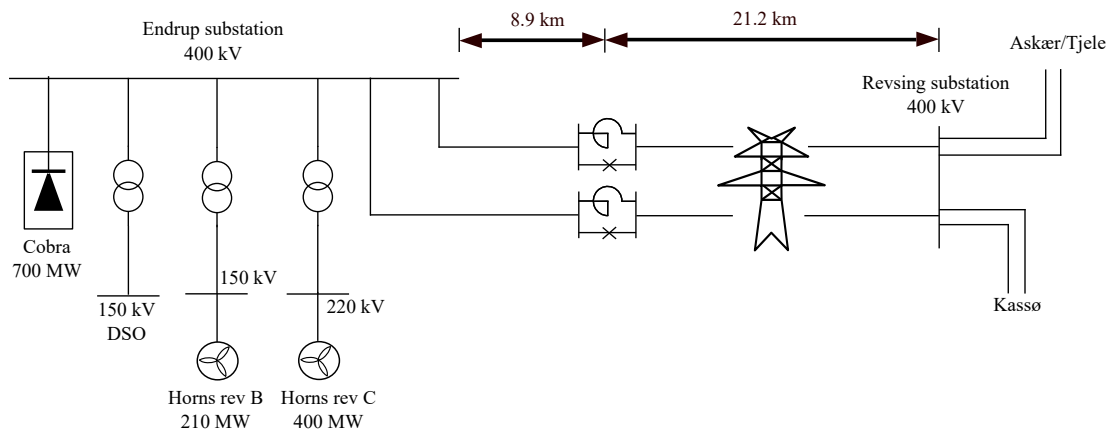

Figure 1.1: Schematic of the 400 kV connection from Endrup to Revsing. [4]

Endrup substation shown in Figure 1.1 is connected to the *High Voltage Direct Current* (HVDC) Cobra system which links Denmark and the Netherlands, as well as two offshore *Wind Turbine* (WT) in Horns rev B and Horns rev C. Furthermore, does the Endrup substation connect to a *Distribution System Operator* (DSO) and the 400 kV substation of Revsing. The transmission line which connects Endrup and Revsing is a double-circuit OHL mounted in a Donau-type lattice tower with a length of 30.1 km [4]. A new substation with a series reactor or PST will be built approximately one-third of the way along the OHL connection from Endrup to Revsing. The series reactor impacts the network by limiting the short-circuit current and providing the ability to control power flow. The series reactors can be bypassed using a *circuit breaker* (CB).

1.2 Power Flow Control: Phase-Shifting Transformer and Series Reactor

In a parallel OHL system, impedances dictate the power flow, with the smallest reactance carrying the largest load. There are techniques for active power flow control: *Phase Shifting Transformers* (PSTs), flexible *Alternating Current* (AC) transmission systems, and series impedance elements such as reactors or capacitors [5]. This project focuses on the use of PST and series reactors as methods for controlling power flow, whose basic principle is considered using the network model of a parallel OHL connection in Figure 1.2.
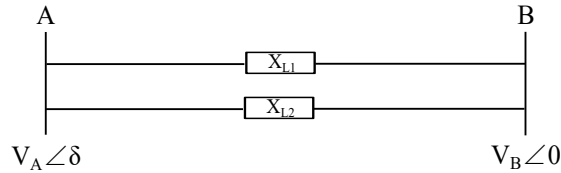
Figure 1.2: Simplified network model of an OHL. [6] [7]

In Figure 1.2, V_A and V_B represent the voltage magnitude at bus A and bus B, with δ representing the phase angle of bus A and 0 representing the phase angle in bus B thus the angle difference between the busses can be considered as δ [6]. Considering the network in Figure 1.2 the active power transferred from bus A to bus B can be defined by Equation (1.1), assuming a lossless system [8].

$$P_s = \frac{V_A \cdot V_B}{X_L} \cdot sin(\delta) \tag{1.1}$$

In Equation (1.1) P_s is the active power which is proportional to the voltage between bus A and bus B, in addition to the phase angle difference. The active power is also

inversely proportional to the line reactance, with the total line reactance of the parallel OHLs in Equation (1.1) represented by X_L. The direction of active power flow of a transmission line between two buses in a power system depends on the phase angle, δ, difference of the voltage [9].

Series reactors control power flow by introducing a controllable line reactance into the transmission line, thereby increasing network impedance. Thus, the series reactor is modelled as a reactance in series with the transmission line [5]. The PST controls power flow by shifting in phase angle δ of the voltage, additionally, increasing the line reactance, which can be contributed to the transformer's leakage reactance [6]. Thus the PST is modelled as a reactance with a phase shift in series with the transmission line. Hence the simplified transmission line circuit in Figure 1.2 with a series reactor or a PST can be modelled as shown in Figure 1.3.
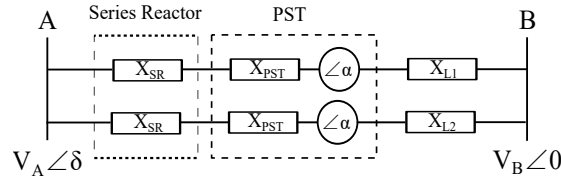
Figure 1.3: Simplified model of an OHL with Series Reactor and PST.

Figure 1.3 shows a simplified model of an OHL with a series reactor and a PST. The active power transfer in Equation (1.1) for the series reactor is defined in Equation (1.2) and the PST is defined as Equation (1.3). [6] [7]

$$P_{SR} = \frac{V_A \cdot V_B}{X_L + X_{SR}} \cdot sin(\delta) \tag{1.2}$$

$$P_{PST} = \frac{V_A \cdot V_B}{X_L + X_{PST}} \cdot sin(\delta + \alpha) \tag{1.3}$$

In Equation (1.2) X_{SR} is the reactance from the series reactor, and in Equation (1.3) X_{PST} is the PST leakage reactance, and α is the phase shifting angle which controls power flow. Mathematically, the addition of either a series reactor or a PST, which are expressed in Equation (1.2) and Equation (1.3) shows that the maximum active power transfer P is lower than the maximum active power transfer before the addition of either component. [6]

1.2.1   Applications in Transmission Networks

Regarding applications of series reactors and PST in transmission networks, are they used in several other countries, which can be referred for series reactor: [5], [10] and for PST: [7], [9], [11]. From the reference [5], the series reactor is utilized in Austria to solve a bottleneck problem in the transmission network. This is achieved by increasing the line impedance within the Austrian network, which shifts the load flow to adjacent lines in neighbouring countries with excess net transfer capacity, thereby solving the bottleneck in the Austrian transmission grid.

The reference [11] describes the application of PST in the Dutch 380 kV grid. The study describes the technical aspect of installing a PST and the operational aspects, including the effect on the power flow from Germany to the Netherlands. The study concluded that the implementation of a PST, if controlled effectively, can allow in principle for an increased capacity and that PSTs are very helpful for European networks to become more predictable and controllable [11].

A comparable study regarding the implementation of either series reactor or PST was conducted in [6]. The study concluded that series reactors reduce short circuit current mainly impacting the transmission line when a fault occurs, but in normal conditions, series reactors limit power flow because of high reactance resulting in higher transmission losses compared to PST with similar power flow. Furthermore, does PTS not reduce the short circuit contribution to the transmission line while still providing power flow control [6].

1.2.2   Impact on Protection System

Energinet's protection philosophy is to have two independent protection relays, with the standard protection scheme consisting of a differential relay and a distance relay [4]. Despite the advantages detailed for the series reactor, it introduces several challenges for the protection scheme. Specifically for distance protection settings of the impedance zones, which are affected by the reactance of the series reactor [12]. Furthermore, in a meshed transmission system, distance protection relies on accurately measuring the voltage and current to compile the impedance, the measurements can be affected by contributions occurring from the HVDC or WT connections.

As distance protection is impedance-based protection the addition of a series reactor will impact the distance protection by changing the impedance. Energinet's proposal of installing a series reactor to the Endrup-Revsing transmission line would be with a CB to bypass the series reactor [4]. Thus, the impedance seen from either Endrup or Revsing towards the transmission line will vary depending on if the series reactor is bypassed or not. Similarly, this is a problem if the PST is installed.

Based on [12], the series reactor impacts the distance protection by under-reaching that causes the relay to not detect within the intended protection zone. Similarly, distance protection encounters issues with under-reaching when used for PST [8]. Consequently, if Energinet's protection philosophy is to be used for the Endrup-Revsing connection then the distance protection's impedance setting becomes inherently important to detect and isolate network fault correctly.

1.3   Problem Statement

The introduction highlighted Energinet's need to implement components for improved power flow control, considering either a series reactor or a PST. Energinet has chosen to implement the series reactor to enhance power flow control and it is likely to become a single-phase $20\,\Omega$ air-core reactor [13]. The implementation of a series reactor in the Endruo-Revsing connection introduces challenges as Energinet's protection philosophy and may not be suitable due to concerns regarding distance protection, which has led to the following problem statement:

How can a suitable protection scheme be developed for the transmission line from Endrup to Revsing in a meshed transmission system considering the integration of a series reactor, ensuring correct fault detection and relay operation?

1.3.1   Methodology

The approach of this project is to review state-of-the-art protection philosophies, focusing on the challenges associated with protecting meshed transmission networks that include series reactors. Additionally, the project will analyze the specific challenges that distance protection encounters if implemented in the system shown in Figure 1.1. In accordance with the findings, a protection scheme with primary and backup protection will be proposed.

Secondly, to validate the proposed protection scheme, a PSCAD model of the $400\,\mathrm{kV}$ Endrup-Revsing system shown in Figure 1.1 will be developed. PSCAD is preferred for the power system studies in this project as it provides accurate *Electromagnetic Transient* (EMT) simulations, which allow for representative analysis of fast transients from the HVDC and WTs. This is crucial when analyzing the impact of the series reactor on relay operation [14]. The model aims to validate the protection system's ability to detect and isolate faults by simulating various fault conditions.

Finally, the results of the simulation will be utilized to asses the viability of the proposed protection system. These will include limitations in the modeling of system components, numerical inaccuracies, or simplifications made during the setup of the simulation in PSCAD.

Chapter 2 State of the Art

This chapter will detail the state-of-the-art review of components impacting the line protection for the Endrup-Revsing connection shown in Figure 1.1, including the series reactor, HVDC-Cobra link, and the *Inverter-Based Resources* (IBRs) from the WTs. The purpose is to assess whether Energinet's standard protection systems with differential and distance protection are viable or if other protection options should be considered when implementing a series reactor.

2.1 Energinet's Standard Protection System

Energinet's protection philosophy is to have two independent protection relays, the standard being a differential relay and a distance relay. The protection system's purpose is to eliminate faults or unacceptable operating conditions for a component and related effects on the network [15]. To achieve protection coordination between the differential relay and distance relay, in Energinet's standard method of protection, protection zones are utilized. The differential relay would be considered as primary protection with a protection zone only covering the protection object. Distance relays will be backup protection and can provide protection coverage to additional objects. The distance protection zones should overlap such that if a fault occurs, overlapping zones would allow more than one set of protection relays to operate with respect to the delay time. The differential relay and distance relay zone protection for a transmission line with a series reactor is shown in Figure 2.1. [13]
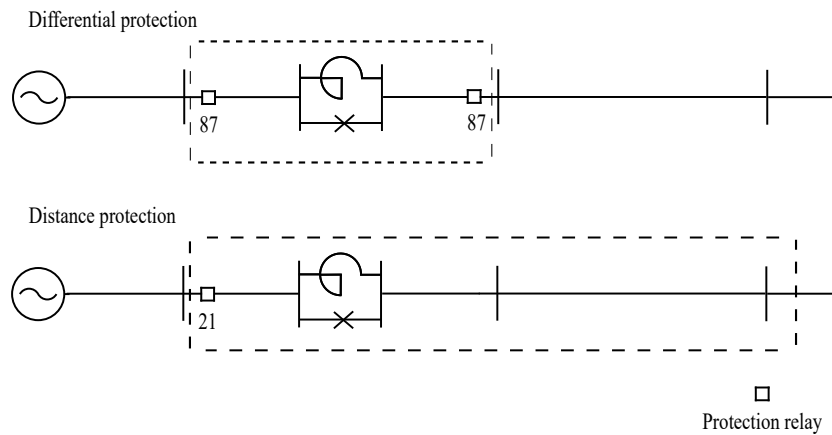
Figure 2.1: Protection zone concept and principle for differential protection and distance protection. [16]

The protection relays in Figure 2.1 are detailed by their ANSI/IEEE standard device numbers, which for the differential relay is 87 and for the distance relay 21. The new substation, which will contain the series reactor, will not have a protection system and will be reliant on the line protection from the Endrup-Revsing connections [13].

7

2.1.1   Differential Protection

Principally, differential protection is based on comparing the current measurement values of the magnitude and phase. The comparison of measured values is based on Kirchhoff's law, which states that the geometric sum of the currents entering or leaving a node must add up to zero at any point in time [17]. Thus, when the differential protection detects a difference in the incoming and outgoing currents exceeding a predefined threshold, the relay trips and isolates the fault. Typically, the measured current values are transmitted to the adjacent relay by fiber optic, as fiber optic has extremely fast communication and has the advantage of being immune to *Electromagnetic Interference* (EMI) from cables, as this is one of the main contributors to the noise [17]. The principle of differential protection of a transmission line is shown in Figure 2.2.
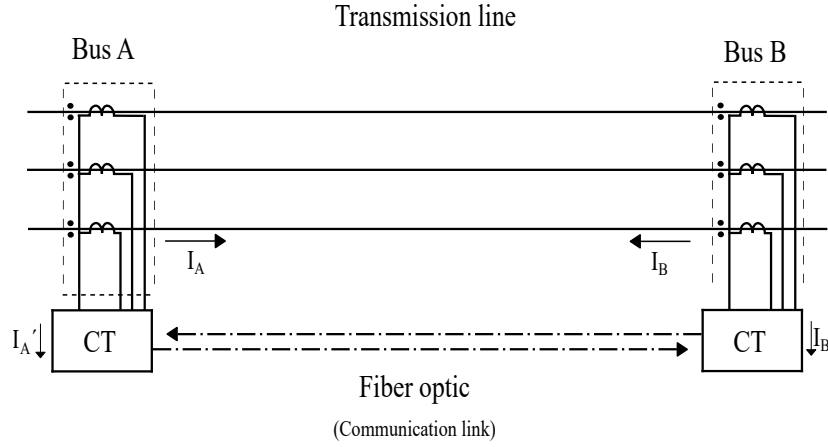
Figure 2.2: Differential protection principle. [18]

In Figure 2.2, the power flow is considered to be flowing from bus A to bus B. Following Kirchhoff's law, the current flowing from the outgoing current in bus A and the incoming current in bus B should be described in Equation (2.1). [18]

$$I_\text{A} + I_\text{B} = 0 \tag{2.1}$$

With I_A and I_B in Equation (2.1) detailing the current and bus A and bus B, respectively. Whenever an internal fault occurs in the transmission line, the differential current in bus A and bus B should be different from zero and can be described as in Equation (2.2). [18]

$$I_\text{A} + I_\text{B} \neq 0 \tag{2.2}$$

The system state in Equation (2.2) exhibits an internal fault as the sum of the currents is different from zero, hence, the relay will operate to isolate the fault. The differential relay will have a threshold current that is different from zero, as this difference

between bus A and bus B only occurs during ideal or lossless conditions. An example of a different relay characteristic is shown in Figure 2.3.
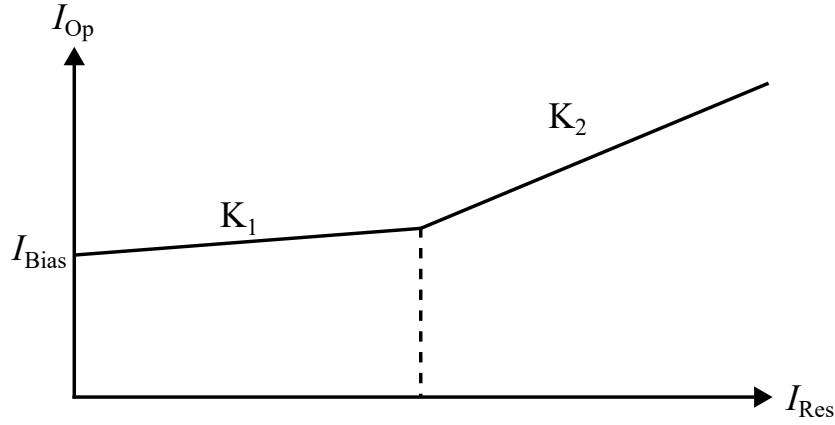
Figure 2.3: Differential protection relay characteristic. [17]

In Figure 2.3, I_{Op} is the current at which the differential protection scheme will operate, while I_{Res} is the restraint current which is set to avoid unnecessary tripping during normal operating conditions, which is set by the I_{Bias} is the threshold current value between the operating and restraint zone. With k_1 and k_2 is the bias factor detailing the steepness for the slope between the restrain and operating zone. The I_{Op} and I_{Res} are defined respectively by Equation (2.3) and Equation (2.4).

$$I_{\text{Op}} = |I_{\text{A}} + I_{\text{B}}| \tag{2.3}$$

$$I_{\text{Res}} = |I_{\text{A}}| + |I_{\text{B}}| \tag{2.4}$$

It is apparent from Figure 2.3 that the pick-up threshold current should be increased when the current throughput increases which is indicated by the two different characteristics for k_1 and k_2. Thus resulting in high sensitivity during load conditions and low-magnitude fault currents while enhancing stability against maloperation during high-current faults, where CT saturation is expected. [17]

When an external fault occurs, the vector sum of the feeder currents is equal to zero, so that no differential current flows in the relay as the current entering and leaving the node is equal to zero. During internal faults, the relay should measure a large differential current between bus A and bus B, thus I_{op} should be larger than the I_{bias}, which will trigger the relay to operate. [17]

2.1.2 Distance Protection

The distance protection determines the state of system operation by measuring the voltage and current, used to compile the impedance which is then compared to the line impedance, used for the distance relay impedance zones. If the measured fault impedance is smaller than the set zone value for the line impedance, an internal fault in the transmission line is detected and the relay should trip [15].

The distance from the relay to the fault location is calculated with the positive-sequence impedance of the line. The reactive part of the line impedance allows the relay to check the distance from the relay to the fault location without taking the fault resistance into account [19]. The distance protection principle is shown in Figure 2.4.
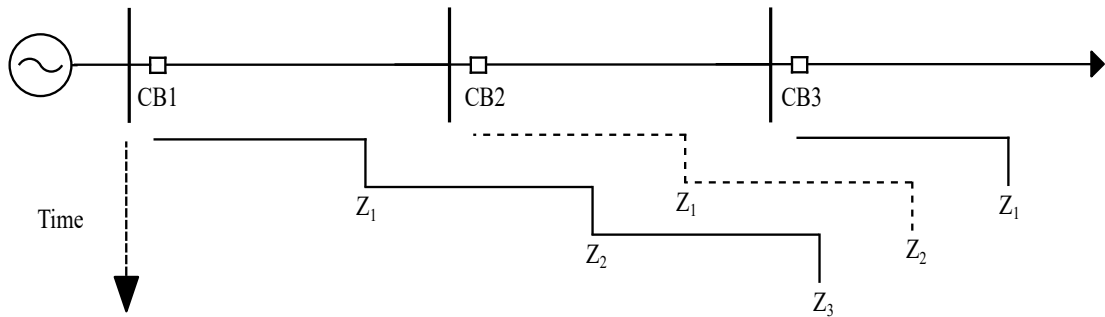
Figure 2.4: Distance protection principle. [15]

Figure 2.4, shows that zone 1 is an under-reaching zone as it does not cover the entirety of the transmission line, typically 80 % of the total length [19]. The remaining transmission line length is covered by an over-reaching zone 2, which is typically set to 120 % of the impedance of the transmission line [19]. The transmission network in Denmark is meshed, which means that distance protection zone setting becomes inherently difficult as the zones are likely to over- or underreach. The distance protection has the tendency to underreach when both lines are energized, and a tendency to overreach when one of the lines is disconnected and earthed at both ends. The distance relay impedance zone settings are detailed in the R-X plane shown in Figure 2.5.
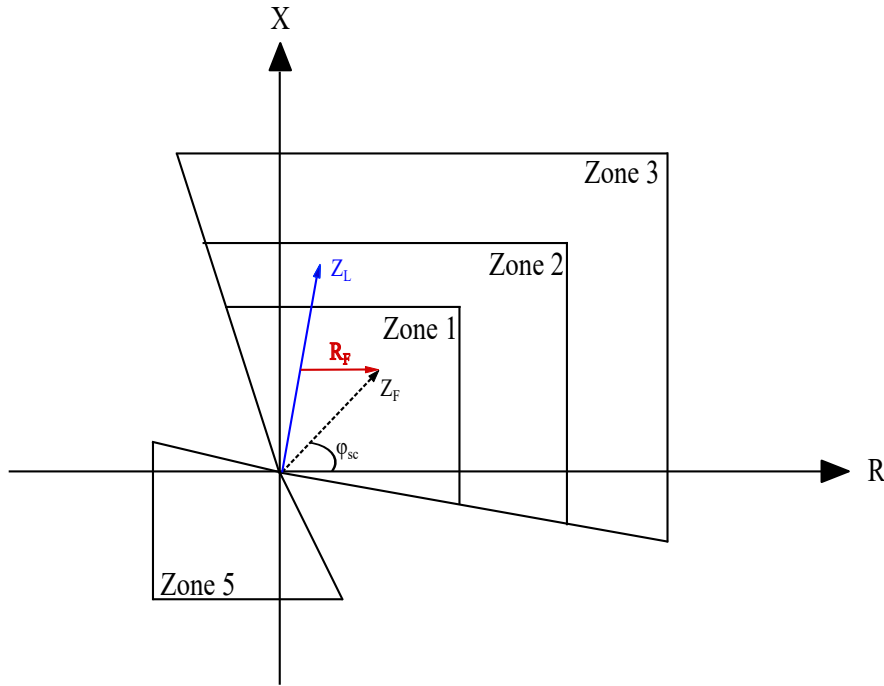
Figure 2.5: Distance protection principle. [15]

Figure 2.5 shows the quadrilateral R-X plane of a distance relay split into four zones, three in the forward direction and a zone in the reverse direction. When a fault occurs, the crossing between the line impedance, Z_L, and the fault resistance, R_F, details the distance to the fault. Z_F details the fault short-circuit fault impedance with φ_{sc} detailing the angle between the short-circuit current and short-circuit voltage. [15]

Permissive Intertrip
To ensure selectivity for distance relays, intertrip, which uses a communication link to send a trip signal from one substation to another, enhances coordination between CBs at both ends of a transmission line. For intertrip, either direct intertrip or permissive intertrip can be used. Direct intertrip utilizes *Direct Underreaching Transfer Trip* (DUTT), which only requires one relay to detect a fault in zone 1 to command both ends to trip the CBs. Thereby, DUTT employs direct tripping without consideration for any protection criteria at the receiving end. Permissive intertrip requires the relay at both ends to detect and confirm a fault for the CBs at both ends to trip. [15]

For permissive intertrip, two options are available: either *Permissive Underreaching Transfer Trip* (PUTT) or *Permissive Overreaching Transfer Trip* (POTT). The PUTT, when detecting a fault in zone 1, will send a permissive signal to the remote relay. The CBs can only trip if the remote relay also detects a fault, thus ensuring two end confirma-

tion before tripping. Instead of using the underreaching zone 1, POTT employs the overreaching zone, either distance protection zone 2 or a zone extension of zone 1, Z_{1B} for fault detection [15]. The zone setting for the permissive intertrip scheme is shown in Figure 2.6.
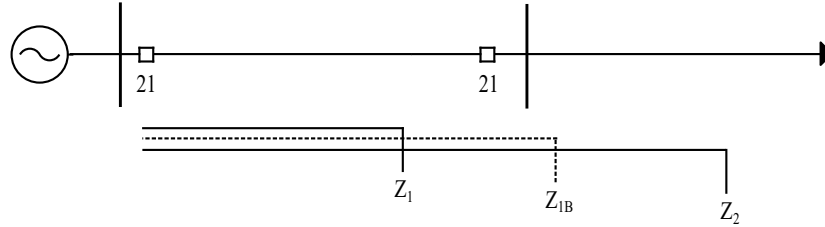
Figure 2.6: Distance protection zones with a zone 1 extension, Z_{1B}. [15]

POTT zone 2, as the permissive overreaching zone, increases the risk of maloperation, as some internal faults will be detected in zone 2. Thereby, the addition of a zone extension of zone 1, Z_{1B}, should theoretically reduce the risk of maloperation, which could be caused by current reversal [15]. The phenomenon of current reversal is further explained in Section 2.3.

DUTT or POTT can advantageously be utilized in systems with weak infeed characteristics where the short-circuit current is not sufficient. In DUTT, the transmission end with sufficient or high short-circuit current contribution detects the fault in zone 1 and directly sends a trip signal to the weak infeed side, ensuring isolation of the fault even if the weak end does not detect the fault due to low current magnitude. In POTT, both relays must confirm the detection of the fault to trip the remote CB. In a system with a weak infeed characteristic, this can be solved by utilizing the echo logic [15]. This modifies the logic of the POTT to allow the weak in-feed end to return the permissive signal as an echo, allowing the strong in-feed end to trip. The strong in-feed relay is then allowed to remotely trip the CB of the weak in-feed end, thereby allowing a direct transfer trip to isolate the fault. [15]

2.2   Series Reactor

Since Energinet is required to have a public tender before buying large-scale equipment, the exact model of the series reactor is still unknown. Energinet has set requirements for the equipment, which are that the series reactor must be a single-phase $20\,\Omega$ air-core reactor [13].

An air-core reactor is considered to be a passive *Fault Current Limiter* (FCL) device as it increases impedance at both nominal and fault current conditions. Whereas active

FCLs have a small impedance at nominal load, which then during fault conditions increases the impedance. [20]

2.2.1 Short-Circuit Characteristics

To asses the impact of the short-circuit contributions of the series reactor the IEC 60909 Standard for calculation the short-circuit current in 50 Hz or 60 Hz three-phase AC systems is applied [21]. The short-circuit current is considered to be the sum of an AC symmetrical component and an aperiodic decaying component. The instantaneous value of the peak short-circuit current, i_p, can be defined in Equation (2.5).

$$i_p = \kappa \cdot \sqrt{2} \cdot I_k'' \tag{2.5}$$

In Equation (2.5), the initial symmetrical short-circuit current, I_k'' is the rms value of the AC symmetrical component of the short-circuit current while κ is a factor given by Equation (2.6). [21]

$$\kappa = 1.02 + 0.98 \cdot e^{-R/X} \tag{2.6}$$

In Equation (2.6), R and X are the real part and imaginary part of the equivalent short-circuit impedance. The decaying aperiodic component of the short-circuit current can be determined as the average between the top and bottom envelope curve of the fault current, as detailed in Equation (2.7). [21]

$$i_{dc} = \sqrt{2} \cdot I_k'' \cdot e^{-2\pi f t \cdot R/X} \tag{2.7}$$

In Equation (2.7), f is the nominal frequency and t is the time. The addition of a passive series reactor will impact the system R/X ratio, which will lead to a lower peak fault current, i_p, and a slower decaying current component, i_d. The waveform of the short-circuit current with a FCL is shown in Figure 2.7.
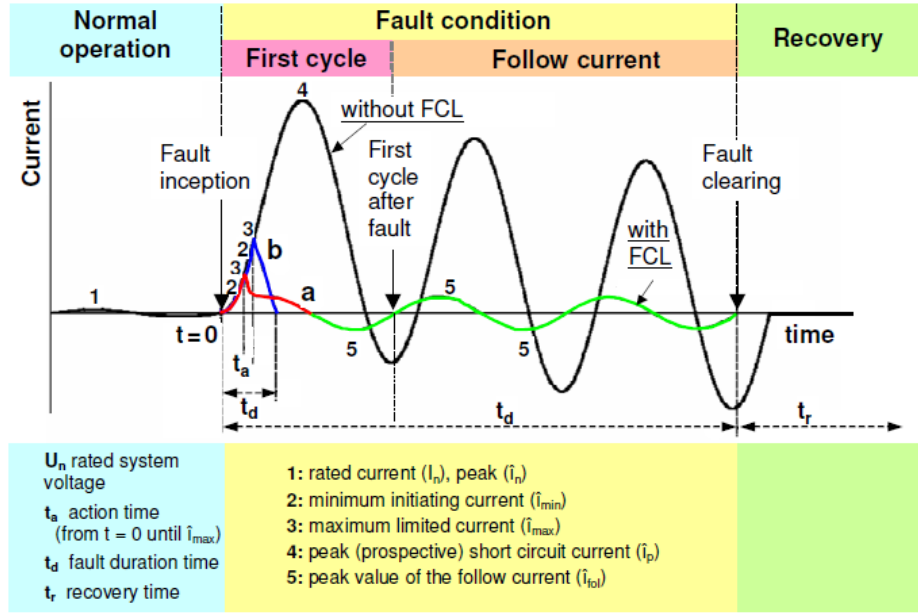
Figure 2.7: Typical current waveform during a fault with a FCL. a: FCL without fault current interruption; b: FCL with fault current interruption. [16]

Figure 2.7 is divided into three main operational phases: normal operation, fault condition, and recovery. At the time $t = 0$, a fault occurs and the waveform distinguishes between two scenarios. Scenario 1, without a FCL, where the short-circuit current rises to a peak value, i_p. In scenario 2, with the FCL, the current is limited, reaching a reduced maximum current, $\hat{i}_{max}$. After the first cycle in the follow current, scenario 2 shows that the FCL maintains its current-limiting function, resulting in a lower peak follow current, $\hat{i}_{fol}$, compared to scenario 1 without an FCL.

It should be noted that scenario 2 with the FCL itself is split into two different scenarios. Scenario 2.a shows the FCL without interruption, and scenario 2.b shows the FCL with interruption.

2.2.2   Impact on Protection System

This section will detail the impact that the series reactor will have on the differential protection and distance protection. The series reactors' impact on differential protection is similar to overcurrent protection. Which is that there is no adverse influence with the condition that the minimum limited fault current still exceeds the threshold for pickup current of the relay. [16]

For distance protection, either a very high or very low X/R ratio can lead to a reduction in accuracy in the impedance determination. This can lead to errors in forward

or backward directional evaluation, thereby leading to maloperation. Therefore, the impact of the impedance must be considered. [16]

2.2.3 Existing Protection System

The reference [10] will be utilized as an example of the successful implementation of series reactors, detailing both the series busbar reactor and series line reactor. The series reactors are 3-phase $12\,\Omega$ air-core outdoor reactors. From the reference, it was found that neither the series bus reactor nor the series line reactor poses any problematic influence on the differential protection. In regards to the protection of the series line reactor, the reference concludes that the zone setting of the distance protection can be adapted such that the series line reactor poses no significant problem to the distance protection. This statement regarding the distance protection in series line reactors is further supported by: [12], [16], [22].

2.3 Protection Considerations with Parallel Transmission Lines

The Endrup and Revsing substations are connected by parallel OHLs, which are defined as two or more circuits of different or equal voltage level that are constructed in the same right-of-way, or utilizing the same transmission tower [23]. This section will address the potential challenges that must be considered for differential and distance protection.

2.3.1 Zero-sequence Impedance

Distance relays determine the distance to the fault by the positive-sequence impedance which is obtained by measuring the voltage and current at the relay location. Therefore, the setting of the distance relay zones is based on the positive-sequence impedance. In the case of a phase fault, the positive-sequence impedance is adequate for locating the fault accurately. However, for ground faults, the positive-sequence impedance alone is insufficient, as the ground distance element does not account for the zero-sequence current effect, leading to potential misoperation [24]. This can be shown if the difference in how the distance relay measures the impedance to ground and phase faults. This is shown in Equation (2.8) for ground faults and Equation (2.9) for phase faults.

$$Z_{\text{ph-g}} = \frac{V_{\text{A}}}{I_{\text{A}} + k \cdot 3I_0} \tag{2.8}$$

$$Z_{\text{ph-ph}} = \frac{V_{\text{A}} - V_{\text{B}}}{I_{\text{A}} - I_{\text{B}}} \tag{2.9}$$

In Equation (2.8), V_{A} and I_{A} are the phase A voltage and current respectively. Similar to Equation (2.9) with the voltage and current values for phase B. In Equation (2.8), $3I_0$ is the residual current, which is the sum of the current from phases A, B, and C defined in Equation (2.10).

$$3I_0 = (I_A + I_B + I_C) \tag{2.10}$$

In Equation (2.8), the zero-sequence compensation factor, k_0 accounts for the complex value included in the relay setting, and can be defined in Equation (2.11). [24] [25]

$$k_0 = \frac{Z_{0L} - Z_{1L}}{k \cdot Z_{1L}} \tag{2.11}$$

In Equation (2.11), Z_{1L} and Z_{0L} are respectively the positive- and zero-sequence line impedance. While k is a constant that can be equal to either 1 or 3, depending on the relay design. [26]

Mutual impedance must be considered in parallel transmission lines. The positive-sequence mutual impedances are very low, thus, their impact on distance relays can be ignored. However, the zero-sequence mutual impedance is significant, and the effect on the distance relays when ground faults occur must be considered [23]. The concept of zero-sequence in a parallel OHL system is shown in Figure 2.8.
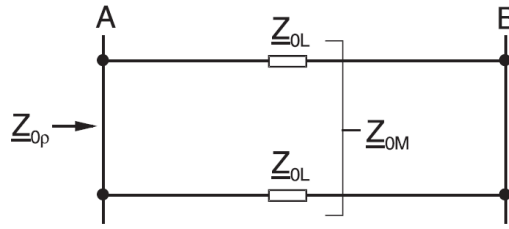
Figure 2.8: Zero-sequence impedance diagram of a parallel OHL system. [23]

In Figure 2.8, Z_{0p} is the double line self-inductance and Z_{0M} is the mutual reactance. The determination of the self- and mutual inductance depends on the tower construction and spacing. The presence of mutual reactance in the zero-sequence network can cause maloperation as a result of the ground distance relay element to either underreach or overreach.

Theoretically, it is possible to compensate for the zero-sequence mutual coupling such that the effect on the reach is minimal. This is accomplished by taking the current from the offending parallel line, I_{RM}, into the ground distance element of the protected transmission line and applying the zero-sequence mutual compensation factor, k_{0M}, to offset the effect of the zero-sequence voltage induced in the protected line [23]. The apparent impedance, Z_{App}, seen by the relay in a parallel transmission line system in p.u. is given by Equation (2.12). [23]

$$Z_{App} = \frac{V_A}{Z_{1L} \cdot (I_A + 3I_0 + k_{0M} \cdot I_{RM})} \tag{2.12}$$

Consequently, distance protection is a viable protection solution for parallel transmission lines with regards to considerations regarding the setting of the projection zones. It is important when setting the protection zones that zone 1 does not overreach due to the zero-sequence mutual and overreaching zones, like Zone 2, should not underreach the remote terminal. [27]

2.3.2 Current Reversal

Current reversal occurs in parallel transmission lines when the fault current changes direction at a bus as a result of a system change, such as a CB operation. The phenomenon of current reversal in POTT, where zone 2 is used as the permissive overreaching zone, is explained using Figure 2.9, where a parallel transmission line system with four CB is considered.
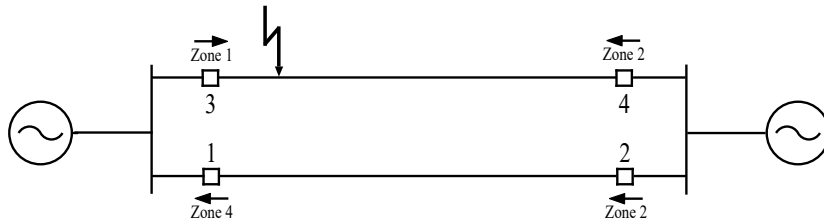
Figure 2.9: Faulted System with all CB closed. [23]

Figure 2.9 shows a fault occurring between CB 3 and CB 4. The relay at CB 3 detects the fault to be in the instantaneous zone 1, which means in POTT because the fault is within zone 2, the relay sends a permissive trip signal to the relay at CB 4. The relay at CB 4 detects the fault within zone 2 but must wait for the permissive signal from CB 3 before tripping. The current reversal occurs if the permissive trip signal never arrives and the fault persists. This means instead of tripping instantly, CB 4 is tripped with the time delay of zone 2.

When the fault occurs, the relay at CB 1 picks up the fault as being in the reverse direction, zone 4, while the relay at CB 2 detects the fault in the forward direction, zone 2. Thus the relay at CB 2 sends a permissive trip signal to the relay at CB 1. The relays will not trip, firstly because of the time delay and secondly because CB 1 rejects that the fault is occurring within zone 1 or zone 2. Figure 2.10 shows the current reversal when CB 3 operates.
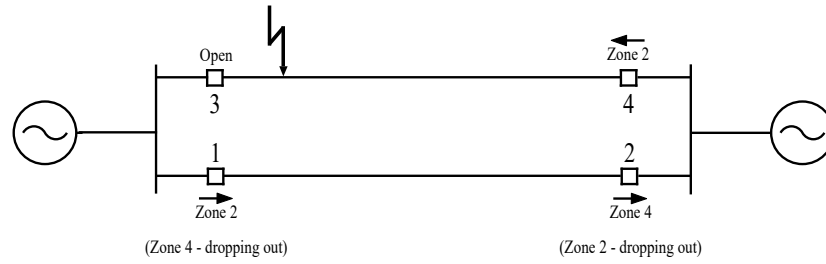
Figure 2.10: Faulted system with CB 3 open. [23]

Figure 2.10 shows that after the CB 3 opens, the fault current redistributes. The re-distribution results in the relays at CB 1 and CB 2 detecting the fault in the opposite direction. This means if CB 1 detects the fault in zone 2, and the received permissive signal from CB 2 does not reset, CB 1 will trip as a result of the current reversal. [23]

This can be solved by the addition of a time delay to the reset mechanism when a fault is detected in zone 4 of the current tripping logic of the distance relay [15]. Another solution is to use the overreaching zone of Z_{1B}, which covers the entire transmission line, such that an internal fault will also be detected in zone Z_{1B} [15]. If this is still a concern, utilizing PUTT is considered to be more secure as it uses the same basic logic as POTT but with an underreaching zone. Underreaching elements are used to key the permissive trip to the remote CB. The remote CB is allowed to trip if it sees the fault as forward with its overreaching element, and the remote end sees it with its underreaching element. Thus, the permissive trip signal is only sent if the fault is within the protected line, which means that there is no danger of misoperation if current reversal occurs. [23]

2.4   Impact on Protection of HVDC Cobra Link

This section will outline the different electrical characteristics exhibited by adjacent HVDC systems compared to traditional HVAC systems and how this impacts protection in HVAC systems. The section will be divided into two sections detailing the HVDC link's impact during steady state and transients.

2.4.1   Steady State

During steady-state operation, the impact of the HVDC Cobra system can be re-garded as that of a constant current source [19]. The cobra link is connected to the AC system using a *Voltage Source Converter* (VSC), which introduces harmonics [28]. Since the VSC utilizes *Pulse Width Modulation* (PWM) to control power flow, it in-troduces high-frequency harmonics into the AC and DC sides of the network. The harmonics generated, while generally at higher frequencies than those produced by conventional *Line-Commutated Converters* (LCC), can still influence AC system opera-

tion and protection schemes [19].

This is not considered to be a problem as most harmonics should be filtered before reaching and disturbing the AC protection system. Nevertheless, under critical conditions, some harmonics will enter the AC network, which could affect the AC protection [19].

2.4.2   Short-Circuit Contributions

When an internal fault occurs in an HVAC system, the short-circuit contribution from an adjacent HVDC system is limited by its VSC, typically constrained to its rated current. The limitation of the fault current infeed from the VSC-HVDC system poses a challenge for the AC protection system. The fault current measured by the protection relay is significantly lower than in traditional systems, which typically provide a higher short-circuit contribution. As a result, this can lead the protection relay to misoperate by failure to detect or isolate the network fault [19].

The short-circuit capability of the HVDC cobra link is limited because of the ability of the *Insulated-Gate Bipolar Transistors* (IGBTs). The typical value of the over-current capability of 1.1 p.u. to 1.15 p.u. of the rated value. It should be noted that the contributions are impacted by the controller's gain, k, and the headband. The deadband is defined as the margin of the voltage drop to which the AC voltage controller is insensitive. [29] [30]

2.4.3   Saturation of Current Transformer

The main concern regarding differential protection is if the CT does not provide accurate measurements of the current. When the CT is operating in the linear range of the magnetizing curve, the measuring error is small and can be neglected [17]. However, when the CT goes into saturation, the measuring error is critical because of the non-linear characteristic of the CT. The HVDC cable discharge current of considerable magnitude, which can be injected into the faulty AC power system through the converter, causing the disturbance. The DC-current component of the fault current can cause the CT saturation. The DC component is created when a fault causes an asymmetrical current waveform. If a DC component is present in the primary current, it will shift the hysteresis curve, causing it to reach the saturation zone on the primary side. This results in an asymmetrical or distorted current measurement on the secondary side of the CT, which can lead to maloperation of the protection relay [19]. The DC component typically decays within 2 or 3 cycles after the fault. A method of mitigating the saturation is to utilize CTs with a high knee-point of the magnetising curve, so that the CT can handle high transient current without saturating [17]. With the decay time of the DC component and that modern numerical protection relays

have filtering, the DC current component is considered not to present a problem [17].

2.5   Short-Circuit Contribution from Wind Turbines

The substation of Endrup has two WT connected, Horns rev B and Horns rev C. To evaluate differential protection and distance protection as a suitable protection scheme, the short-circuit contributions from the WT must be considered. In regards to short circuit contributions, WTs can be split into four main categories, which are listed below and shown in Figure 2.11. [31] [32]

- *WT type A:* Fixed speed WT, shown in Figure 2.11a.

- *WT type B:* Partial variable speed WT with variable rotor resistance, shown in Figure 2.11b.

- *WT type C:* Variable speed WT with partial-scale frequency converter, also known as *Doubly-Fed Induction Generator* (DFIG)-based WT. Type C WT is shown in Figure 2.11c.

- *WT type D:* Variable speed WT with full-scale power converter, also known as *Voltage Source Converter* (VSC)-based WT. Type D WT is shown in Figure 2.11d.

(a) Fixed speed WT with directly grid-connected squirrel-cage induction generator.

(b) Partial variable speed WT with variable rotor resistance.

(c) Variable speed WT with partial scale power converter.

(d) Variable speed WT with full-scale power converter.
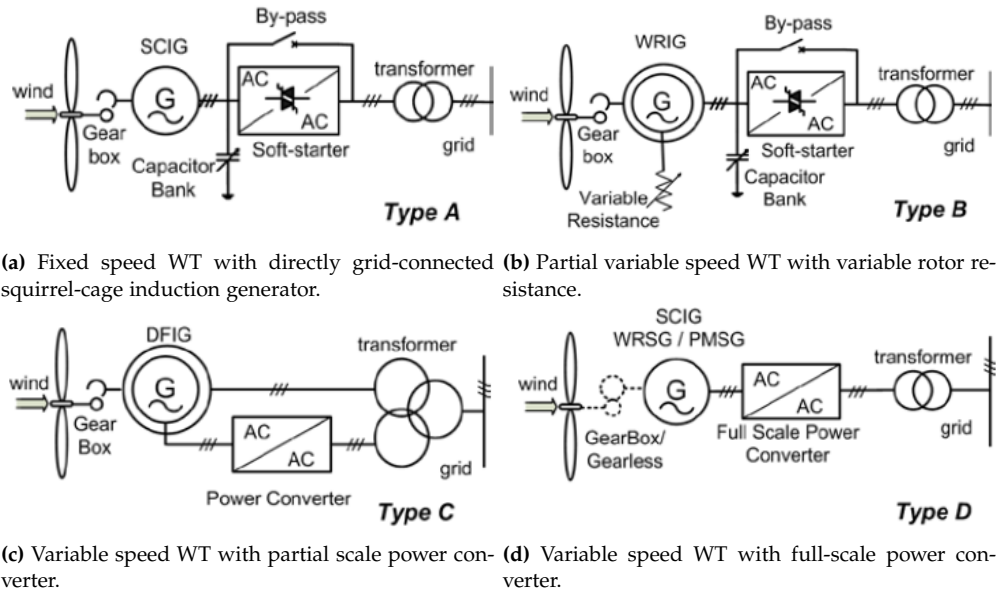
Figure 2.11: WT concepts. [32]

Horns Rev B utilizes the Siemens SWT 2.3-93 turbine model, classified as a Type C WT. Horns Rev C uses the MHI Vestas V164-8.3 MW turbine model, which is

categorized as a Type D WT [13]. Therefore, this project is limited to considering the short-circuit contributions from WT type C and type D.

2.5.1 Type C - Doubly Fed Induction Generator

In a synchronous generator, the magnetic field is maintained by the field current in the rotor winding, so it can continue supplying voltage during a fault. As for the WT type C the induction generator of the DFIG relies on magnetizing flux that weakens during a fault, causing the fault current to decrease quickly and not last as long. Figure 2.12 illustrates the short-circuit current contributions of WT Type C for different fault types. The waveforms are derived from the IEEE study presented in [33].

The three-phase to ground fault (3LG) in Figure 2.12 shows a significant transient component, characterized by the initial peak which is followed by a decaying oscillation. The faulted phase currents exhibit a rapid reduction before stabilizing. The line-to-line to ground fault shows an asymmetric response where the faulted phases, phase A and phase B, experience a current increase, while the non-faulted phase, phase C, remains relatively unaffected. The transient oscillations still decay over time, which is longer than the three-phase fault when compared. The single-line-to-ground fault shows a fault in phase A, which has a lower current contribution compared to the two previous cases. The transient response gradually dampens, on a similar time period as the line-to-line to ground fault. [33]

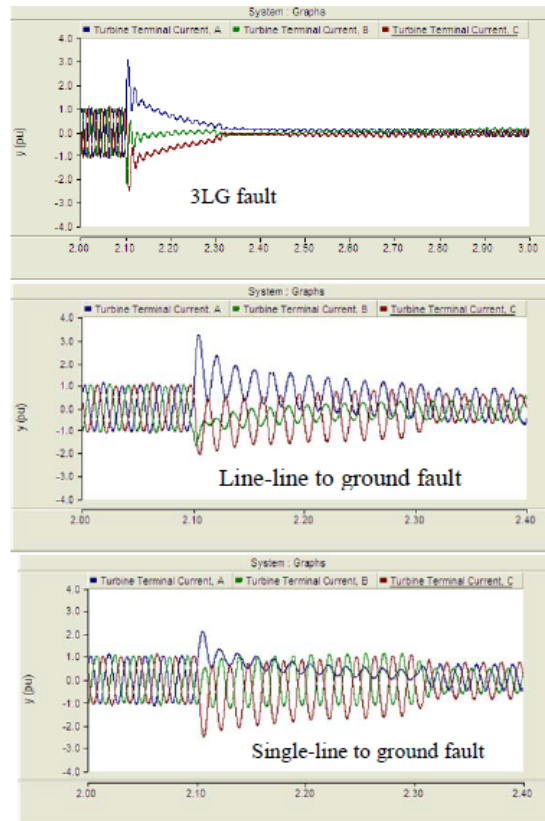**Figure 2.12:** Short-circuit current of a Type C WT for different fault types. [33]

The general tendency of the short-circuit response shown in Figure 2.12 presented in [33] is shared by other studies. Other studies include [34], [35], [36], where both balanced and unbalanced faults were considered, with both the short-circuit contributions and the system impact on frequency and voltage detailed for the type C WT.

2.5.2   Type D - Full Converter Wind Turbine Generator

The short-circuit contributions of the Type D WT are controlled by the DC/AC grid-side converter, limiting the maximum fault current to a value slightly above the rated current [21]. This is shown in Figure 2.13, as presented in [33].

In Figure 2.13, the three-phase to ground fault (3LG), which shows, contrary to the type C WT in Figure 2.12, that the type D WT exhibits a more controlled and stable fault current response with no significant transient current components. Line-to-line to ground fault shows a similar controlled response, with all three phase currents exhibiting nearly symmetrical oscillations. The single-line-to-ground fault indicates that the current contribution remains within a controlled range, with minimal unbalanced behavior between phases. The short-circuit currents of the WT type D have a longer decay time than the WT type C.

Similar tendencies are shown for the type D WT in regards to the short-circuit characteristics in the studies: [21], [32], [37].
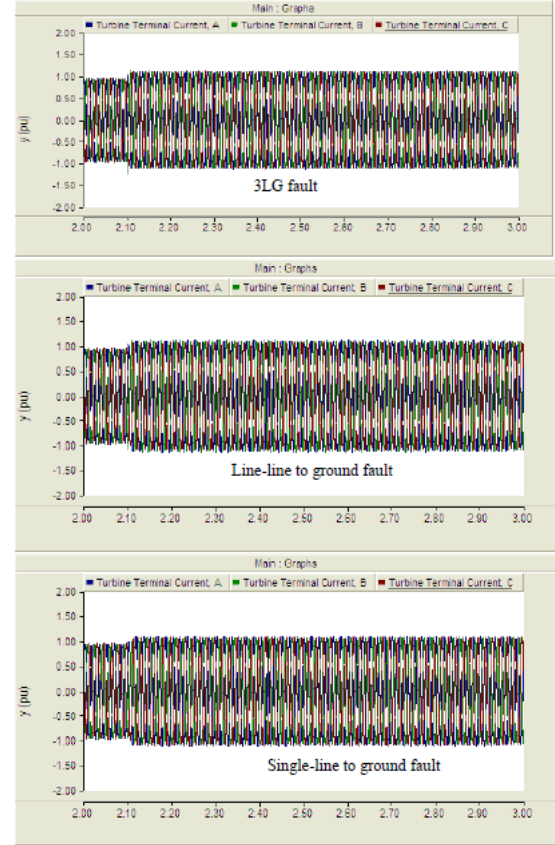
Figure 2.13: Short-circuit current of a Type D WT for different fault types. [33]

It should be noted that the exact short-circuit contribution from WT type C and type D depends on the power converter algorithm [33]. Therefore, while the analysis provides a general understanding, it should be taken as a general estimation based on the citations provided in Section 2.5. However, generally WT type C and type D have different short-circuit characteristics compared to synchronous generators. The initial peak current is lower, and the decay time is much shorter. Therefore, the sensitivity setting of the protection system is important, as it should be able to detect faults even when the fault current contribution from the in-feed is limited.

Chapter 3 PSCAD Modelling

This project aims to validate the protection system for the Endrup to Revsing transmission line with a series reactor. This chapter will outline the necessary transmission system modelling of the general system shown in Figure 1.1. This will be completed by conducting simulations to asses the short-circuit contributions and the response of the protection system. This chapter will therefore include all components utilized for the PSCAD simulation.

3.1 PSCAD Model

This section will detail the modelling and settings of the PSCAD components, which include the infeed characteristics, measuring systems, transmission lines, and series air-core reactor. The PSCAD model is shown as a single-line diagram in Figure 3.1.
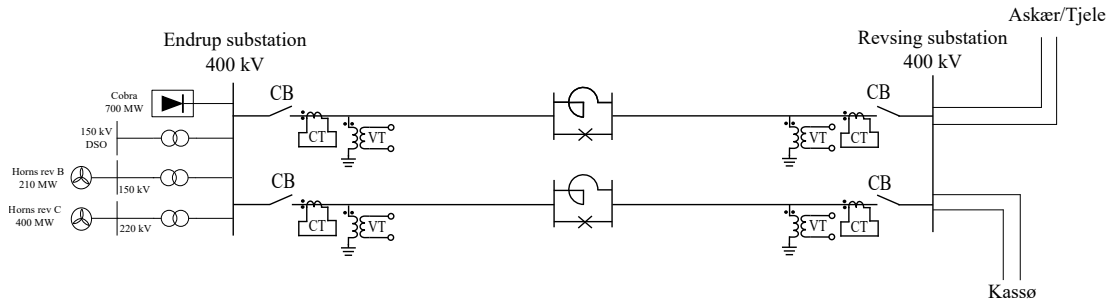
Figure 3.1: PSCAD model.

Figure 3.1 does not display the protection system as it will be built using metathetical blocks in PSCAD. The built protection system will utilize the CTs and VTs measurements to control the state of the CBs. The following sections will detail the transmission lines, the line reactor, and the infeed characteristics of Endrup.

3.2 Transmission Line

In this section, the transmission line modelling will be detailed. The transmission lines include the Endrup-Revsing connection and any grid connection from Revsing further upstream in the network, limited to one substation.

3.2.1 Transmission Line: Endrup-Revsing

The Endrup-Revsing connection is a parallel 3-phase system. Physically, the system consists of six conductors with two ground wires on a Donau transmission tower. The PSCAD modelling of the transmission line tower between the substation of Endrup and Revsing is shown in Figure 3.2.
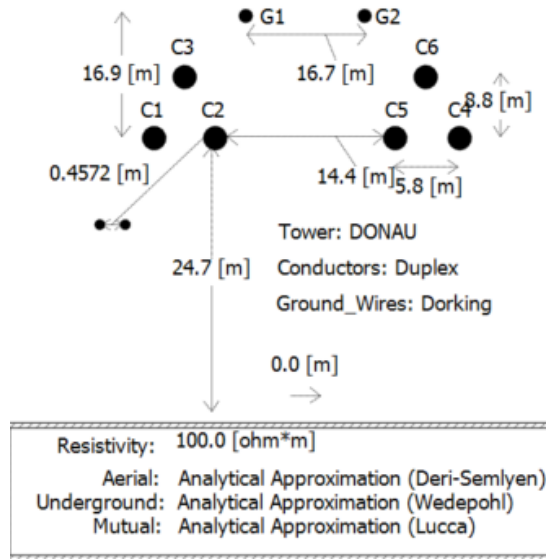
Figure 3.2: Transmission tower measurements, for the Endrup to Revsing connection.

Figure 3.2 shows the transmission line tower modelling details, including the distances between conductors and ground wires. This is important as it impacts the system impedance. The data required for modelling the conductor and ground wire are detailed in Table 3.1.

Table 3.1: The parameters used for modelling of the parallel OHL system from Endrup to Revsing in PSCAD.

Parameter		Endrup-Revsing
Rated Voltage		400 kV
Frequency		50 Hz
Conductors		3
Configuration		Trefoil
	Number	2
	Configuration	Flat
	Spacing	0.4572 m
Sub-conductor	Type	Solid
	DC-Resistance	0.0422 Ω/km
	GMR	16.4025 mm
	Outer radius	17.2435 mm
	Type	Solid
	DC-Resistance	0.2982 Ω/km
Ground Wire	GMR	7.3021 mm
	Outer radius	7.6765 mm

3.2.2 Transmission Line: Kassø-Tjele

The transmission line from Kassø to Tjele also connects to Revsing and Askær. The connection is a parallel system that shares a transmission line tower. A single-line diagram of the connection from Kassø to Tjele is shown in Figure 3.3.
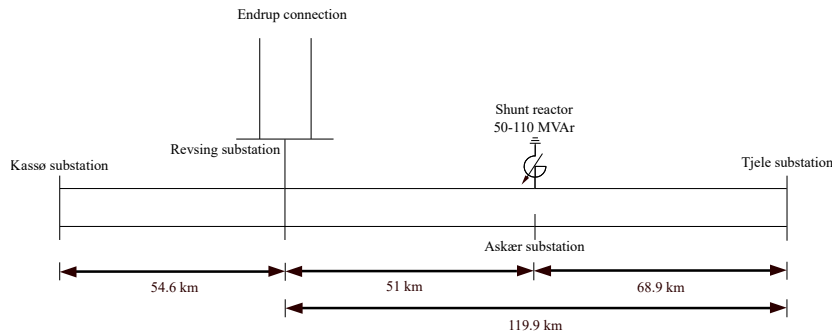
Figure 3.3: Single-line diagram from Kassø to Tjele.

In Figure 3.3, the connections from Kassø to Tjele are all OHLs consisting of Donau transmission towers. Figure 3.4 shows the transmission line tower type and configurations with measurements.
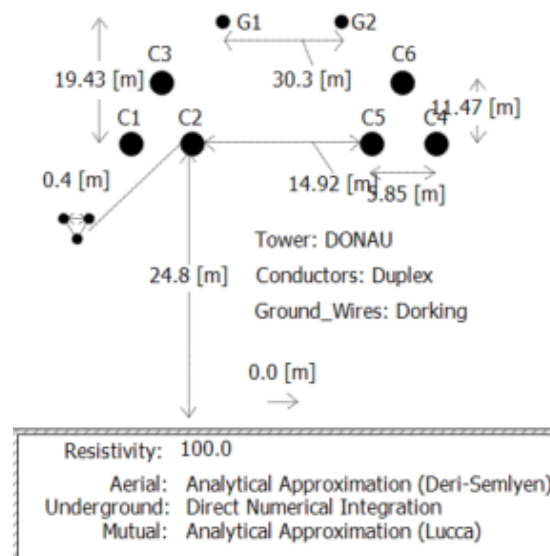
Figure 3.4: Transmission tower measurements, for the Kassø to Tjele connection.

The modelling of the conductors and ground wires is shown in Table 3.2.

Table 3.2: The parameters used for modelling of the parallel OHL system form Kassø to Tjele in PSCAD.

Parameter		Kassø-Tjele
Rated Voltage		400 kV
Frequency		50 Hz
Conductors		3
Configuration		Trefoil
Sub-conductor	Number	3
	Configuration	Trefoil
	Spacing	0.4 m
	Type	Solid
	DC-Resistance	0.0334 Ω/km
	GMR	17.1810 mm
	Outer radius	18.0850 mm
Ground Wire	Type	Solid
	DC-Resistance	0.2982 Ω/km
	GMR	7.3021 mm
	Outer radius	7.6765 mm

3.3   Air-Core Reactor

This section will detail the modelling of the series air-core reactor in PSCAD. For modelling the air-core reactor in series with the transmission line in PSCAD, there are the following options: saturable reactor, hysteresis reactor, or linear reactor.

The saturable reactor and the hysteresis reactor are both predefined blocks in PSCAD. The saturable reactor includes a nonlinear magnetic saturation, and the hysteresis reactor includes the hysteresis curve and eddy current effects. These characteristics are why the saturable reactor and hysteresis reactor are typically used for iron-core reactors, as they include nonlinear effects, which are important when modelling the iron-core. As neither of these effects is relevant for the air-core reactor, the linear reactor will be utilized for the study. The linear reactor, on which the air core reactor will be based on, can be accurately modelled with a linear inductor in series with a resistance. The inductance and resistance values are detailed in Figure 3.3.

Table 3.3: Settings for the modelling of the air-core reactor.

Settings	Air-core reactor
Inductance	0.0636 H
Resistance	0.01 Ω

The resistance in Table 3.3 is present to add stability to the simulation in PSCAD of

the air-core reactor. The specific value is chosen as it does not impact the system in a steady state while providing the necessary stability. The inductance in Table 3.3 has been calculated utilizing Equation (3.1).

$$X_L = 2\pi f \cdot L \tag{3.1}$$

Where X_L is $20\,\Omega$ and the frequency is $50\,\text{Hz}$.

3.4 Cobra-link

The cobra link is an HVDC cable connection between Denmark at Endrup's substation and the Netherlands at Eemshaven substation. A reference model of an HVDC link with a bipole topology, half-bridge submodules, and a hybrid DC breaker is utilized to obtain the characteristic. The model is explained in [38] and is shown in Figure 3.5.
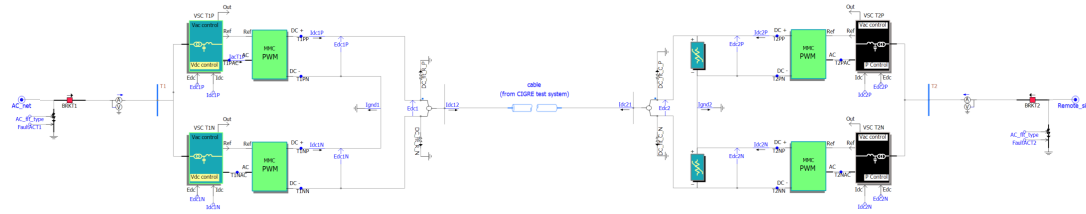
Figure 3.5: The HVDC cobra link modelling.

Figure 3.5 shows the HVDC link model. The model's right side is the remote end, which is connected to a three-phase voltage source that produces $700\,\text{MW}$ at a nominal voltage of $400\,\text{kV}$. The AC voltage is converted into DC and transmitted 325 kilometers to the local end, which converts the DC voltage into AC and is then connected to the grid at Endrup. The information regarding the cobra connection is detailed in [39].

During the integration of the HVDC model in Figure 3.5, a problem was encountered when faults were induced in the Endrup to Revsing transmission line. Whenever an unbalanced fault was induced, the model would provide inaccurate and unexpected results, as this could cause an imbalance in the current output injected into the transmission network. This phenomenon did not occur in the original model whenever a fault was induced on the remote or local AC side, nor if balanced faults were induced. This was solved by overwriting some of the restrictions on the model's output and changing the control parameters. This has slightly changed the short-circuit output for the unbalanced faults, which is further discussed in Section 4.1.

3.5   Wind Turbines

The WTs utilized for this project will be PSCAD reference models. The reference models for the WT can be found in [14]. This section will be limited to detailing the input parameters of the WTs and will not include an in-depth explanation of the models.

3.5.1   Horns Rev B

As specified in Chapter 2, Horns Rev B is a type C WT. The PSCAD reference model contains two parts: mechanical and electrical systems. The mechanical system consists of a WT and a pitch angle controller. The electrical system consists of a grid-side converter and controls, a rotor-side converter and controls, DC-link chopper protection, crowbar protection, and a low-pass filter. The schematic of the *Wind Turbine Generator* (WTG) type C model in PSCAD is shown in Figure 3.6.

Figure 3.6: A PSCAD reference model for the type C WTG. [14]

The model's mechanical and electrical parts, shown in Figure 3.6, are further explained in [14]. The input parameters for the WTG model are shown in Table 3.4.

Table 3.4: Input parameters of the Type C WTG model.

Settings	WT type C
Nominal frequency	50 Hz
AC voltage magnitude	150 kV
Rated active power	210 MW
Input wind speed	11 m/s

3.5.2 Horns Rev C

Horns Rev C consists of type D WTs, as described in Chapter 2. The PSCAD reference model, similar to the type C WT, consists of a mechanical and an electrical system. The mechanical system is configured with a WT and a pitch angle controller, while the electrical system consists of a grid-side converter and controls, a machine-side converter and controls, DC-link chopper protection, low pass filters, a transformer, and a scaling component that increases the WTG's power level to model equivalent wind farm. The WT type D model is shown in Figure 3.7.
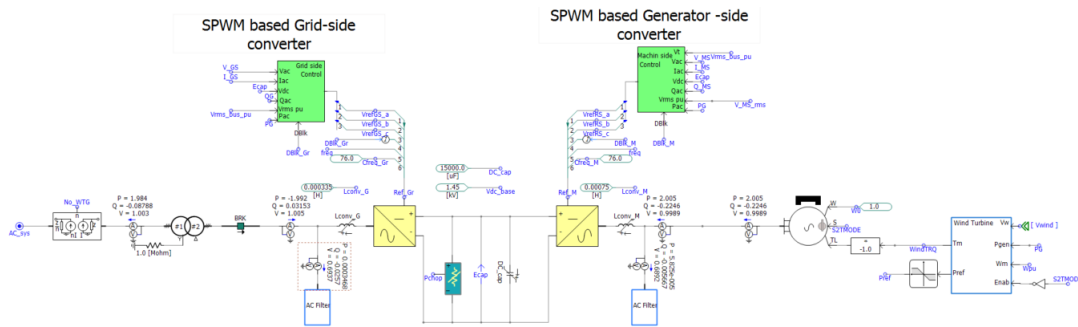
Figure 3.7: A PSCAD reference model for the type D WTG. [14]

The model's mechanical and electrical parts, shown in Figure 3.7, are further explained in [14]. The input parameters for the WTG model are shown in Table 3.5.

Table 3.5: Input parameters of the Type D WTG model.

Settings	WT type D
Nominal frequency	50 Hz
AC voltage magnitude	220 kV
Rated active power	400 MW
Input wind speed	11 m/s

3.6 Protection System

This section will detail the limitations of the protection system that will be simulated in PSCAD. Furthermore, this section includes an explanation of how the protection system in PSCAD functions and the protection system's settings.

3.6.1 Protection System Limitation

The transmission line protection that will be utilized for this project is Energinet's standard method, which consists of differential and distance protection. The protection system is shown in the radial system in Figure 3.8.
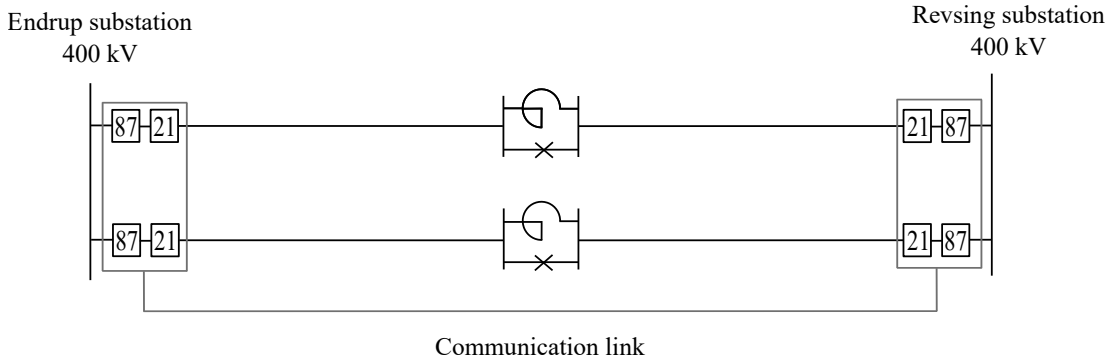
Figure 3.8: Protection system modelling, which includes the PSCAD schematic.

Figure 3.8 shows the protection system which Energinet wants to utilize for the Endrup to Revsing connection. As Chapter 2 has outlined, differential protection does not encounter problems with measuring errors of the CTs. This project will, due to time limitations, be limited to considering settings and validations on distance protection.

3.6.2   PSCAD: Distance Protection

In PSCAD, distance protection modelling relies on mathematical blocks and equations. This section will, therefore, detail how the distance protection is built and configured. The distance protection model is explained utilizing the distance protection at Endrup. The model is shown in Figure 3.9.
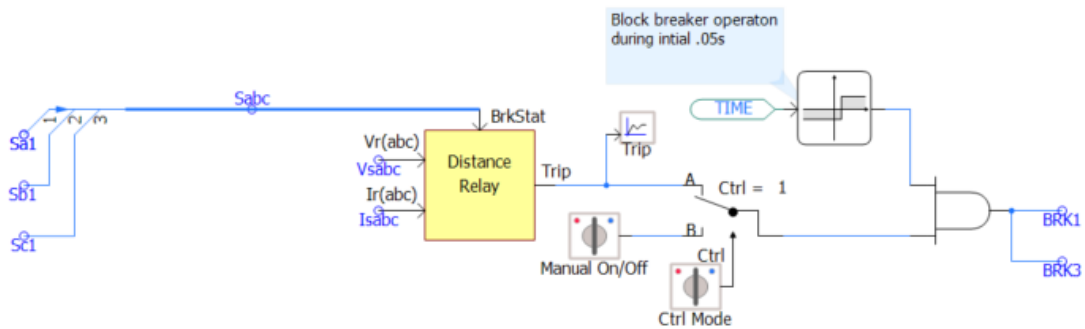
Figure 3.9: Schematic of distance protection in PSCAD.

The input for the distance relay sub-module is the voltage and current measurements at the Endrup end of the transmission line. The voltage and current measurements of V_{sabc} and I_{sabc} are the secondary side measurements obtained from the VT and CT, whose schematic is shown in Figure 3.10.

(a) Schematic of VT in PSCAD.

(b) Schematic of CT in PSCAD.

Figure 3.10: Instrument transformers in PSCAD.

The instrument transformers in Figure 3.10 are utilized in PSCAD to include the DC offset and CT saturation. The ratio of the CT is 1500/1 A, while the ratio of the VT is 400kV/100 V.

The initial step of the distance protection is to utilize *Fast Fourier Transform* (FFT) to eliminate high-frequency components during faults or transients. The FFT requires the base frequency of 50 Hz and the initial measurements obtained for the instrument transformers shown in Figure 3.10. This is shown for the voltage in Figure 3.11.
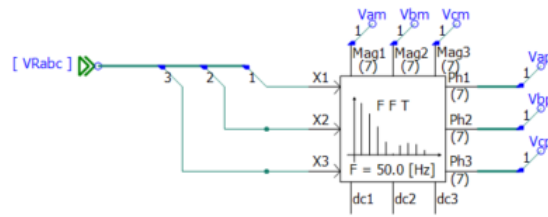
Figure 3.11: FFT voltage model.

Similarly, the FFT is utilized for the current measurements, which is shown in Figure 3.12. Additionally, the current measurements include the magnitude and angle of the zero sequence current.
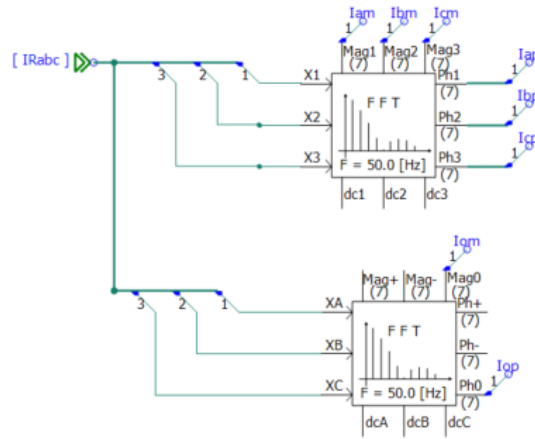
Figure 3.12: FFT current model.

The output measurements from the FFT blocks are utilized to calculate the impedance. Figure 3.13a and Figure 3.13b are utilized to calculate the phase-to-phase and phase-to-ground impedance, respectively.
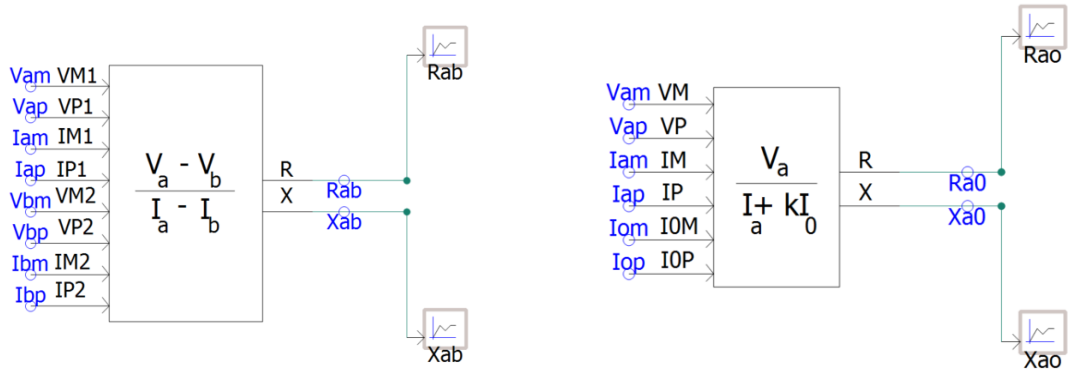
(a) Calculation of the impedance for the phase A to phase B fault.

(b) Calculation of the impedance for phase A to ground faults.

Figure 3.13: Equations used for the distance relay to calculate the impedance for phase-to-phase and phase-to-ground faults

Figure 3.13a shows the impedance calculation between phase A and phase B, while Figure 3.13b shows the impedance calculation of phase A to ground. It should be noted that this calculation is to be completed between all phase configurations and all phases to ground. The measurements from the impedance calculation are then compared with the zone settings values of distance relays utilizing the block in Figure 3.14.
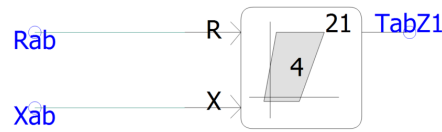
Figure 3.14: The block logic utilized for the zone setting of the distance protection in PSCAD.

The zone setting block shown in Figure 3.14 is for the phase-to-phase impedance between phase A and phase B. It should be noted that these settings should be configured for all phase-to-phase and phase-to-ground configurations. The measurement of T_{abZ1} is then a part of the trip logic shown in Figure 3.15.
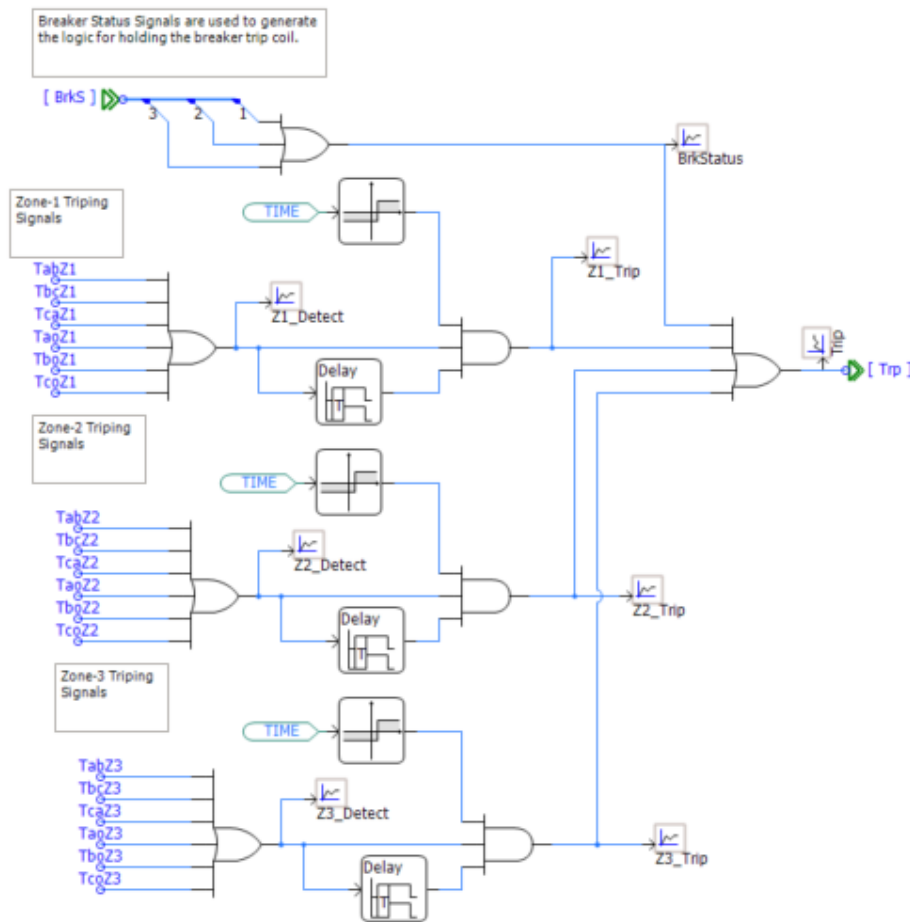
Figure 3.15: The block logic utilized to send the trip signal distance protection in PSCAD.

The trip logic in Figure 3.15 shows how the trip signal is processed for faults in zone 1 and zone 2. Firstly, the T_{abZ1} signal is processed in an or-block such that any phase-to-phase or phase-to-ground fault can trip the relay. Leaving the or block is

the detection signal, which then enters an and-block, which includes a time delay; such a time delay between zone 1, zone 2, and zone 3 tripping can be achieved. The signal that leaves the and-block is the tripping signal, which enters an or-block such that both tripping signals from zone 1, zone 2, and zone 3 faults can trip the relay.

3.6.3   Energinet's Standard

This section will briefly detail Energinet's standard setting of the impedance zones and time delays for the distance relay, which will be applied for this project. [13]

- Zone 1: $70 - 90\% \cdot Z_{\text{line}}$. Time delay of 0 seconds.

- Zone 2: $0.85 \cdot (Z_{\text{line}} + 0.85 \cdot Z_{\text{adjacent line}})$. The adjacent line is the shortest adjacent transmission line. Time delay of 0.3 seconds.

- Zone 3: $1.2 \cdot (Z_{\text{line}} + 0.85 \cdot Z_{\text{adjacent line}})$. Time delay of 0.8 seconds.

- Zone 5: Emergency protection, 3-6 transmission lines (backwards). Time delay of 2.5 seconds.

3.6.4   Impedance Setting

This section will detail the distance relay impedance setting. There will be two different sets of impedance settings, which are based on the state of the air-core reactor. If the air-core reactor is bypassed, it will have no impact on the transmission line impedance and should, therefore, be disregarded. If the current is flowing through the air-core reactor, the impedance should be considered for the setting values of the distance relay. The transmission line data for the Endrup to Revsing connection is outlined in Table 3.6.

Table 3.6: Data for the Endrup to Revsing transmission line obtained through PSCAD

Transmission line data: Endrup - Revsing	Ω/km
Positive sequence resistance, R_1	0.02324
Positive sequence reactance, X_1	0.28889
Zero-sequence resistance, R_0	0.16793
Zero-sequence reactance, X_0	0.83396
Mutual zero-sequence resistance, R_{m0}	0.14186
Mutual zero-sequence reactance , X_{m0}	0.36867

Table 3.6 specifies the transmission line data in Ω/km, the transmission line is in total 30.1 km with the air-core reactor located 8.9 km from the Endrup substation. Thus, for both the distance relays in Endrup and Revsing, the air-core reactor is located in zone 1. Similarly to Table 3.6, Table 3.7 details the transmission line data for the Kassø to Tjele connection.

Table 3.7: Data for the Kassø to Tjele transmission line obtained through PSCAD

Transmission line data: Kassø - Tjele	Ω/km
Positive sequence resistance, R_1	0.01223
Positive sequence reactance, X_1	0.26685
Zero-sequence resistance, R_0	0.15513
Zero-sequence reactance, X_0	0.80277
Mutual zero-sequence resistance, R_{m0}	0.13923
Mutual zero-sequence reactance , X_{m0}	0.38333

To calculate the impedance settings of the distance relay, Equation (3.2) and Equation (3.3), to calculate the compensation k_0. [40]

$$\frac{R_E}{R_L} = \frac{1}{3} \cdot \left(\frac{R_0}{R_1} - 1 \right) \tag{3.2}$$

$$\frac{X_E}{X_L} = \frac{1}{3} \cdot \left(\frac{X_0}{X_1} - 1 \right) \tag{3.3}$$

The compensation factor is important to account for the current flowing through the earth in phase-to-ground faults. Therefore, during a phase-to-ground fault, the term $k_0 \cdot I_0$ compensates for the current flowing through the earth. This can also be applied to the mutual earth factor k_{m0}, which can be calculated using Equation (3.4) and Equation (3.5). [40]

$$\frac{R_M}{R_L} = \frac{1}{3} \cdot \left(\frac{R_{M0}}{R_1} - 1 \right) \tag{3.4}$$

$$\frac{X_M}{X_L} = \frac{1}{3} \cdot \left(\frac{X_{M0}}{X_1} - 1 \right) \tag{3.5}$$

Equation (3.2) through Equation (3.5) is utilized to calculate the compensation factor k_0 and k_{m0} for the two transmission line configurations.

Impedance Setting: 1. Air-core Reactor Bypassed
The length of the Endrup to Revsing connection is 30.1 km, and the shortest adjacent line to Revsing is 51 km. The connections from Endrup further downstream in the network are unknown; therefore, the distance relay at Revsing will be based on the calculation made from the substation of Endrup. This will give the accurate values for zone 1, while the zone 2 and 3 settings in Revsing are not an accurate representation. The impedance zone settings are detailed in Equation (3.6) through Equation (3.11).

Zone 1:

$$R_{\text{reach,prim}} = 0.02324\Omega/\text{km} \cdot (30.1\,\text{km} \cdot 0.85) = 0.5946\,\Omega \qquad (3.6)$$

$$X_{\text{reach,prim}} = 0.28889\Omega/\text{km} \cdot (30.1\,\text{km} \cdot 0.85) = 7.3913\,\Omega \qquad (3.7)$$

Zone 2:

$$R_{\text{reach,prim}} = 0.85 \cdot ((0.02324\Omega/\text{km} \cdot 30.1\,\text{km})$$
$$+ 0.85 \cdot (0.01223\Omega/\text{km} \cdot 51\,\text{km})) = 1.0452\Omega \qquad (3.8)$$

$$X_{\text{reach,prim}} = 0.85 \cdot ((0.28889\Omega/\text{km} \cdot 30.1\,\text{km})$$
$$+ 0.85 \cdot (0.26685\Omega/\text{km} \cdot 51\,\text{km})) = 17.2240\Omega \qquad (3.9)$$

Zone 3:

$$R_{\text{reach,prim}} = 1.2 \cdot ((0.02324\Omega/\text{km} \cdot 30.1\,\text{km})$$
$$+ 0.85 \cdot (0.01223\Omega/\text{km} \cdot 51\,\text{km})) = 1.4756\Omega \qquad (3.10)$$

$$X_{\text{reach,prim}} = 1.2 \cdot ((0.28889\Omega/\text{km} \cdot 30.1\,\text{km})$$
$$+ 0.85 \cdot (0.26685\Omega/\text{km} \cdot 51\,\text{km})) = 24.3162\Omega \qquad (3.11)$$

The impedance zone settings calculated in Equation (3.6) through Equation (3.11) comply with Energinet's standard setting method for distance protection outlined in Section 3.6.3. The setting values are outlined in Table 3.8 with the time delay.

Table 3.8: The primary side impedance setting for the distance relay at Endrup, where the air-core reactor is bypassed.

Grading (Reach)	$+R_{\text{reach,prim}}[\Omega]$	$+X_{\text{reach,prim}}[\Omega]$	Time delay [s]
Zone 1	0.5946	7.3913	0.0
Zone 2	1.0452	17.2240	0.3
Zone 3	1.4756	24.3162	0.8

The impedance zone setting outlined in Table 3.8 is shown in Figure 3.16, with the addition of the impedance of the OHL connection.

Figure 3.16: The distance protection zones for the impedance setting 1.

Impedance Setting: 2 Air-core Reactor Included

The impedance setting when the air-core reactor is included in series with the OHL introduces an additional impedance. The reactor, with an inductance of $0.0636\,\text{H}$, introduces an additional primary reactance $X_{\text{reach,prim}}$ of $20\,\Omega$. Additionally, the series air-core reactor contributes to the primary resistance $R_{\text{reach,prim}}$ by $0.01\,\Omega$. The impedance setting with the air-core reactor included is detailed in Table 3.9.

Table 3.9: The primary side impedance setting for the distance relay at Endrup, where the air-core reactor is included.

Grading (Reach)	$+R_{\text{reach,prim}}\,[\Omega]$	$+X_{\text{reach,prim}}\,[\Omega]$	Time delay [s]
Zone 1	0.6046	27.3913	0.0
Zone 2	1.0552	37.2240	0.3
Zone 3	1.4856	44.3162	0.8

In Table 3.9, Energinet's standard, detailed in Section 3.6.3 can not be utilized as this will give underreaching zones. Therefore, instead of utilizing the value of Z_{line}, the desired distance must be used. Hence, the zone calculation for zone 1 is as outlined in Equation (3.12) and Equation (3.13).

$$R_{\text{reach,prim}} = (0.02324\,\Omega/\text{km} \cdot (30.1\,\text{km} \cdot 0.85)) + 0.01\,\Omega = 0.6046\,\Omega \qquad (3.12)$$

$$X_{\text{reach,prim}} = (0.28889\,\Omega/\text{km} \cdot (30.1\,\text{km} \cdot 0.85)) + 20\,\Omega = 27.3913\,\Omega \qquad (3.13)$$

The impedance zone setting outlined in Table 3.9 is shown in Figure 3.17, with the addition of the impedance of the OHL connection.

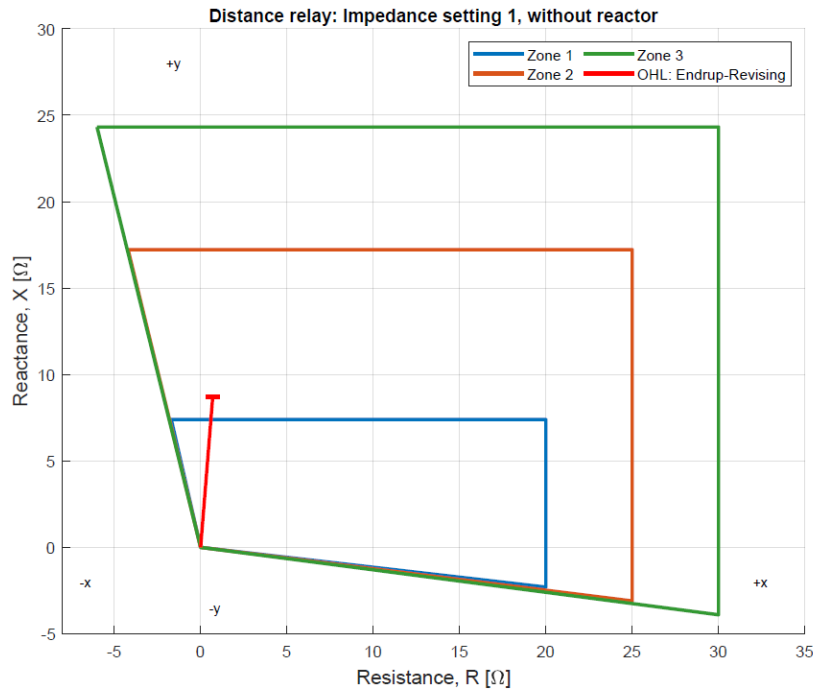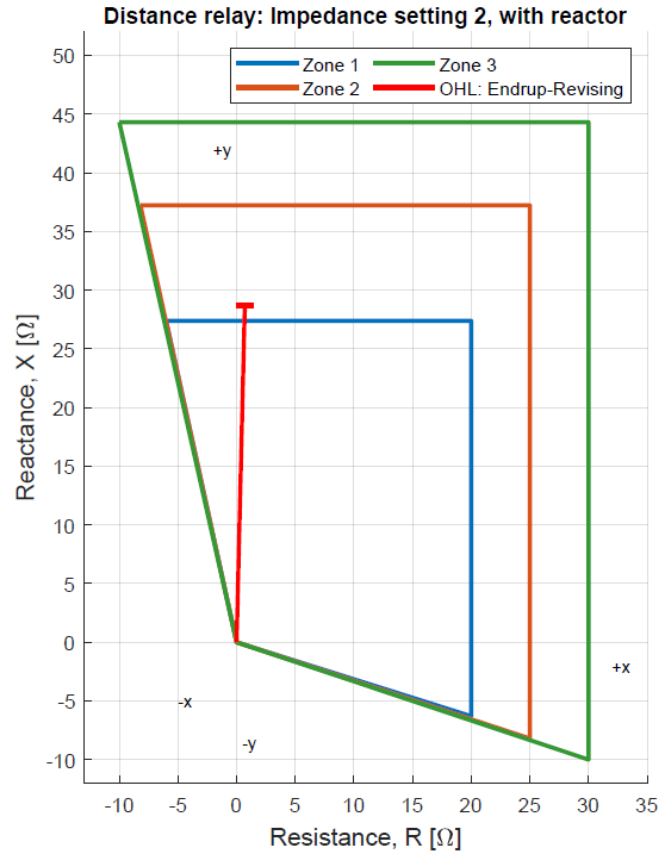**Figure 3.17:** The distance protection zones for the impedance setting 2.

Thus concluding Chapter 3, it should be noted that the secondary side impedance for the impedance zones is calculated and outlined in Appendix A.

Chapter 4 PSCAD Simulations

This chapter will include the PSCAD simulation results of various cases to asses the distance protection and its impedance setting of the zones. The purpose of this chapter is to asses the distance protections ability to identify and isolate network fault. To obtain this the chapter will firstly asses the voltage and power characteristics in Endrup followed by the short-circuit current contributions. Secondly, the distance protection will be tested with different fault types, fault resistances and locations of the fault.

4.1 Verification of Models

This section will include an assessment of the models of the two WTs and the HVDC-link regarding both the steady state output power and voltage, and the current contributions during a fault event. This assessment will be based on a comparison between the short-circuit current contributions obtained from PSCAD and the theoretical short-circuit contributions outlined in Chapter 2. Note that all short-circuit current contritions which will be presented in the section is with a fault impedance of $0.1\,\Omega$.

4.1.1 Wind Turbine Type C

The specifications of the WT type C are outlined in Table 3.4. Figure 4.1 shows voltage and power output for the WT type C, which are measured at the output of the WTG and the POC at Endrup.
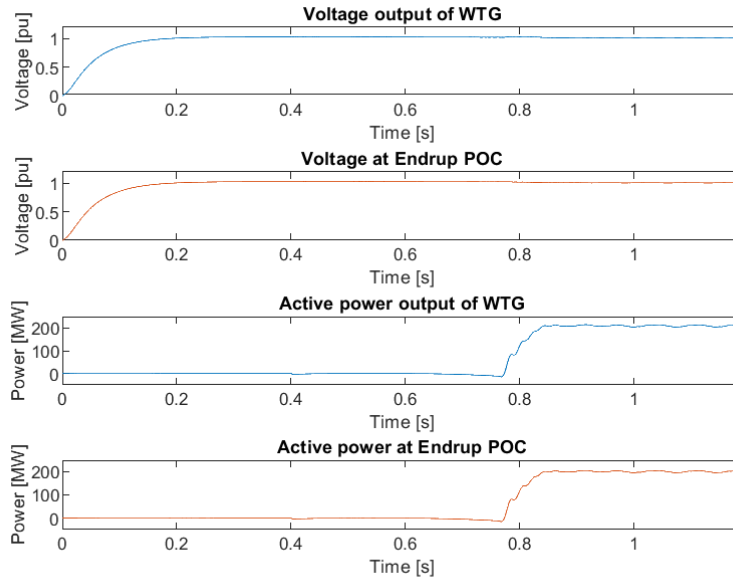
Figure 4.1: The voltage and active power from the WTG output and POC at Endrup.

Figure 4.1 shows that the voltage and power are ramped up during the initialization. The voltage and power are within the desired limits, both at the WGT output and the POC at Endrup. Therefore, is the WTG post 1 second considered operating within acceptable limits and in steady state. The short-circuit current contribution from the WT 3 is shown in Figure 4.2.
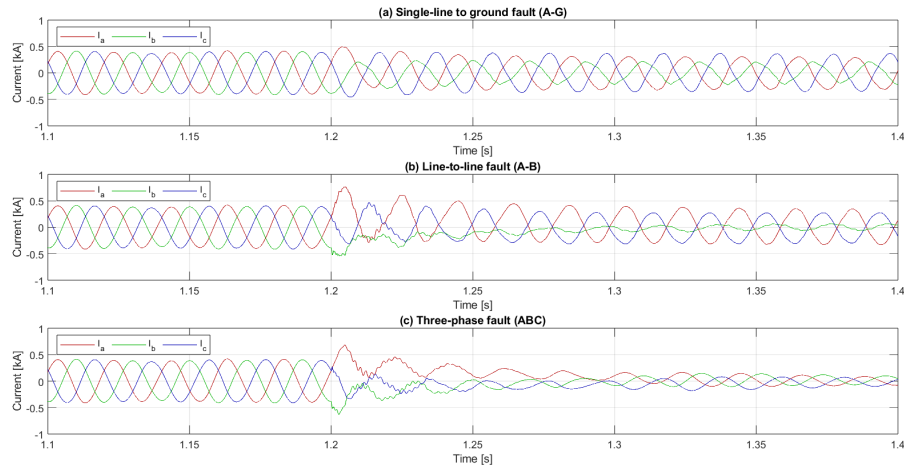
Figure 4.2: Short-circuit current contributions when a fault is induced in the Endrup to Revsing transmission line.

Figure 4.2 shows the expected short-circuit current characteristics when compared to the expected short-circuit contributions of three different fault types in Figure 2.12. Figure 4.2 shows that all fault types initially peak in the first few cycles post the fault event at 1.2 seconds, which depends on the fault type. When compared to expected short-circuit current contributions and characteristics outlined in Figure 2.12, Figure 4.2

4.1.2   Wind Turbine Type D

The specifications of the WT type D are outlined in Table 3.5. Figure 4.3 shows voltage and power output for the WT type C which are measured at the output of the WTG and the POC at Endrup.
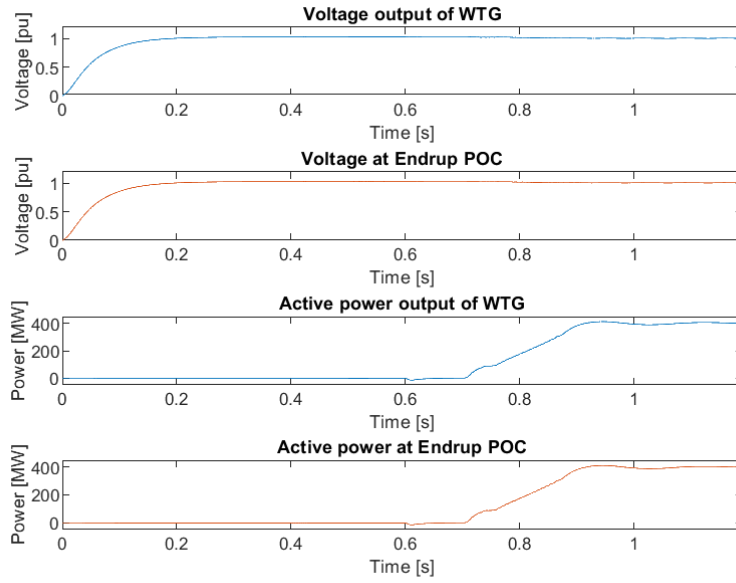
Figure 4.3: The voltage and active power from the WTG output and POC at Endrup.

Figure 4.3 shows the voltage and power output from WT type D. The voltage is initialized similar to WT type C in Figure 4.1, while the power initialization differs. This can be attributed to the difference in control methods, which also impacts the single-line to ground short-circuit current contributions of WT type D shown in Figure 4.4.
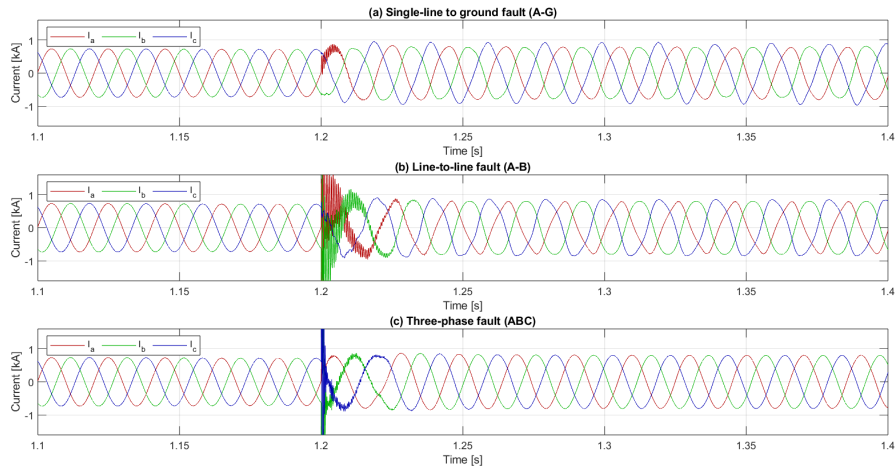
Figure 4.4: Short-circuit current contributions when a fault is induced in the Endrup to Revsing transmission line.

Figure 4.4 shows the short-circuit current contribution of three different fault types. Figure 4.4, when compared to the expected short-circuit contributions in Figure 2.13 shows the expected contribution. There is no significant initial peak, but the phases where the fault occurs are distorted when the fault occurs at 1.2 seconds. The short-circuit current is higher than the steady-state current, which is shown pre-fault. In the case of a single-line to ground and line-to-line to ground faults, there is an imbalance between phases post-fault, which is shown in Figure 4.4, and can be attributed to the control of the converter.

4.1.3   HVDC Cobra Link

This sections details the voltage and power output of the HVDC cobra link and the short-circuit contributions during faults in the Endrup-Revsing transmission line. Firstly is the voltage and power input and output shown in Figure 4.5.
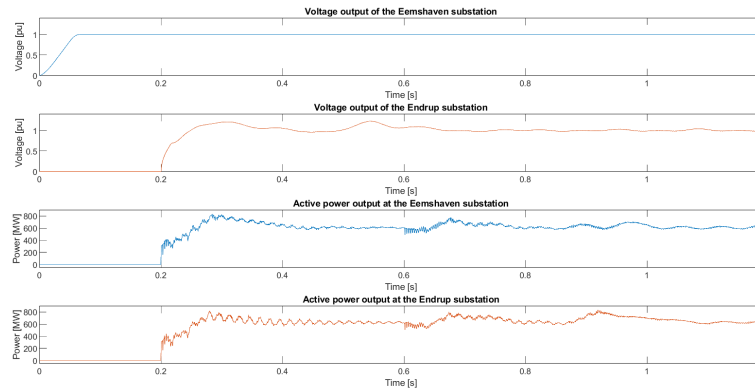
Figure 4.5: The voltage and active power from the HVDC at the remote end of Eemshaven and the local end of Endrup.

In Figuer 4.5 the voltage input measurement is taking form the grid side connection in Eemshaven substation while the power is the measurements from the DC side of the substation. While the voltage and power output of the Endrup substation is taking from the AC-side cobra link. Figure 4.5 shows that the voltage and power both are ramped up to the operational limits. The voltage and power varies within acceptable limits as the VSC regulates the output voltage magnitude and phase to reach steady-state. Secondly, the short-circuit current contribution is shown in Figure 4.6.
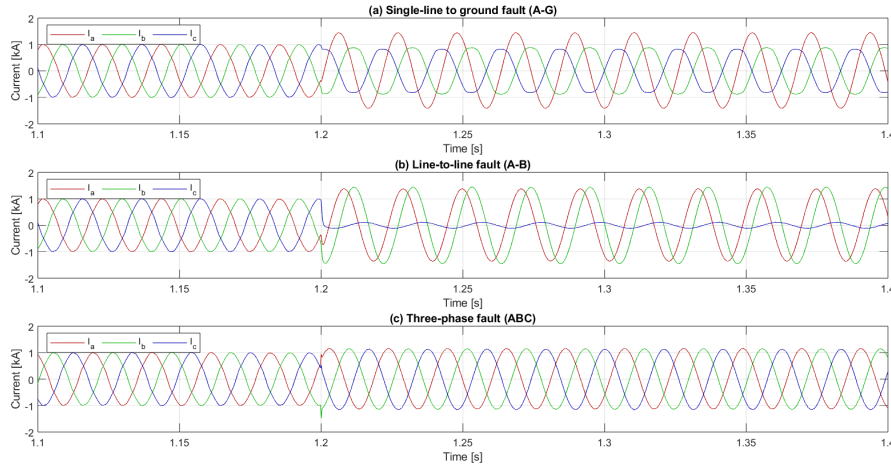
Figure 4.6: Short-circuit current contributions when a fault is induced in the Endrup to Revsing transmission line by the HVDC at the remote end of Eemshaven and the local end of Endrup

Figure 4.6 shows that the nominal current is approximately 1 kA in steady-state, in the time range of 1.1 to 1.2 seconds. The faults are induced at the time of 1.2 seconds in the simulations. For the single-line to ground fault is the magnitude of the fault current is approximately 1.3 kA, the line-to-line to ground fault is approximately 1.45 kA, and the three-phase to ground fault is approximately 1.2 kA. The higher fault current contributions of single-line to ground and line-to-line to ground faults compared to the three-phase to ground fault can be attributed to the reactive power injections from the cobra link due to the imbalance between the three phases.

To summarize, the short-circuit current contributions of the WT type C, WT type D, and the HVDC cobra link have shown acceptable results. The WT type C and WT type D have been compared with the expected results outlined in Chapter 2, while the HVDC cobra link current controller is limited to provide 1.5 p u of the nominal current.

4.2 Simulation Cases for the Distance Protection

This section will detailed the different protection cases which will be investigated in PSCAD. The protection cases will be split into two groups: case I.X and case II.X. Case I will utilize the impedance setting 1, where the air-core reactor is bypassed, and case II will utilize impedance setting 2, where the air-core reactor is included. X details the fault location which is outlined in Table 4.1.

Table 4.1: Explanation of the fault cases which will be tested in PSCAD.

Case number	Fault location	Fault impedance	Protection zone
Bypass: Series air-core reactor			
Case I.1	Endrup-Revsing: 4.5 km	0.1 Ω	Zone 1
Case I.2	Endrup-Revsing: 19.5 km	0.1 Ω	Zone 1
Case I.3	Revsing-Askær: 10 km	0.1 Ω	Zone 2
Case I.4	Revsing-Askær: 40 km	0.1 Ω	Zone 3
Including: Series air-core reactor			
Case II.1	Endrup-Revsing: 4.5 km	0.1 Ω	Zone 1
Case II.2	Endrup-Revsing: 19.5 km	0.1 Ω	Zone 1
Case II.3	Revsing-Askær: 10 km	0.1 Ω	Zone 2
Case II.4	Revsing-Askær: 40 km	0.1 Ω	Zone 3

Table 4.1 details the fault cases that will be tested in PSCAD. Each fault location is associated with a case number and should be interpreted in accordance with the following example for case I.1: the fault will be induced 4.5 km from Endrup substation in the direction towards the Revsing substation. Each fault location is related to an impedance zone of the distance relay. The impedance setting outlined in Section 3.6.1 should for zone 1 reach 25.6 km of the Endrup to Revsing transmission line, zone 2 reaches 21.6 km of the Revsing to Askær transmission line, and zone 3 reaches 61.8 km of the Revsing to Tjele transmission line, which is equal to the Revsing to Askær transmission line plus an additional 10.8 km. As the shunt reactor in Askær is not considered in this protection study, the fault is induced in the Revsing to Askær transmission line.

Case I.1 and case I.2 are both faults which occurs in zone 1 but on different sides of the series air-core reactor, similarly to case II.1 and case II.2. This is expected to have a limited impact on the results obtained in case I.1 and case I.2. However interesting in case II.1 and case II.2 as this will detail if the series air-core reactor impacts the distance relays abilitto measure the impedance to the fault accurately.

The fault impedance in all simulation cases is 0.1 Ω, which means that the short-circuit current contributions in Section 4.1 are representable for the simulation cases outlined in Table 4.1.

4.2.1 Simulation 1: Fault Detection

This section will detail the results of the fault detection simulation, which will analyze the distance relays' ability to detect and isolate faults based on the settings outlined in Section 3.6. The distance relay will be tested where both the series air-core reactor is bypassed and included.

In the simulation, the distance to the fault is measured using the reactance, as it provides the most accurate estimate [15]. The results of fault cases I and II with the series air-core reactor bypassed and included are outlined in Table 4.2, with the fault cases explained in Table 4.1.

Table 4.2: Results from the fault cases I and II, when the series air-core reactor is bypassed and included.

		Measured impedance [Ω]	Corresponding distance [km]	%Error	Trip Time [s]	Fault detected zone	Assessment
Bypass: Series air-core reactor							
Single-line to ground fault	Case I.1	1.42	4.92	+10.56	0.25	Zone 1	Approved
	Case I.2	6.15	21.29	+9.17	0.27	Zone 1	Approved
	Case I.3	12.31	43.65	+8.86	0.56	Zone 2	Approved
	Case I.4	21.75	79.03	+12.74	1.01	Zone 3	Approved
Line-to-line fault	Case I.1	1.21	4.19	-5.84	0.26	Zone 1	Approved
	Case I.2	5.41	18.73	-3.96	0.23	Zone 1	Approved
	Case I.3	11.20	39.49	-1.51	0.58	Zone 2	Approved
	Case I.4	18.89	68.31	-2.55	1.04	Zone 3	Approved
Three-phase fault	Case I.1	1.26	4.36	-2.02	0.25	Zone 1	Approved
	Case I.2	5.38	18.62	-4.50	0.24	Zone 1	Approved
	Case I.3	10.96	38.59	-3.76	0.53	Zone 2	Approved
	Case I.4	19.02	68.80	-1.86	1.02	Zone 3	Approved
Including: Series air-core reactor							
Single-line to ground fault	Case II.1	1.43	4.95	+10.10	0.25	Zone 1	Approved
	Case II.2	26.91	25.15	+5.95	0.25	Zone 1	Approved
	Case II.3	32.78	47.15	+6.08	0.56	Zone 2	Approved
	Case II.4	41.20	78.82	+5.57	1.01	Zone 3	Approved
Line-to-line fault	Case II.1	1.22	4.22	-5.37	0.24	Zone 1	Approved
	Case II.2	24.98	17.92	-1.69	0.25	Zone 1	Approved
	Case II.3	30.70	39.35	-0.65	0.53	Zone 2	Approved
	Case II.4	38.75	69.52	-0.40	1.02	Zone 3	Approved
Three-phase fault	Case II.1	1.24	4.29	-3.67	0.26	Zone 1	Approved
	Case II.2	25.01	18.03	-1.57	0.24	Zone 1	Approved
	Case II.3	30.79	39.69	-0.35	0.54	Zone 2	Approved
	Case II.4	38.81	69.75	-0.24	1.02	Zone 3	Approved

Table 4.2 presents the results of fault cases I and II, where three different fault types: single-line to ground, line-to-line, and three-phase faults, were used to assess the distance relay. When evaluating the trip time and the zone in which the fault is detected, the simulation results align with expectations and support the approved assessment of the relay's operational performance. However, the measured impedance of the single-line to ground shows that the relay measures a higher impedance than expected, thus overestimating the distance to the fault. While the line-to-line and three-phase faults measured impedance slightly lower than expected, thereby underestimating the distance to the fault slightly. This applies to both fault cases I and II. However, fault case II shows a more accurate estimation of the distance to the fault, which can be attributed to the higher impedance corresponding to a lower error in the measurement reading of the exact impedance reach. This also applies to the discrepancies in the measurement errors between the line-to-line and three-phase faults in cases I and II. The fault location measured in fault case I by the distance relay in the R-X plane is shown in Figure 4.7.

Figure 4.7: Fault impedance measured by the distance protection in PSCAD, where the series air-core reactor is bypassed, Case I.

Figure 4.7 shows the data outlined in Table 4.2 for the measured impedance in case

I when the series air-core reactor is bypassed. Table 4.2 has shown that there is an overestimation of the distance to the fault by 8.8 % to 12.7 % for the single-line to ground fault when the series air-core reactor is bypassed and 5.5 % to 6.1 % for fault occur beyond the series air-core reactor when included. Thus, both simulation shows the same tendency as the relay overestimates the distance of the single-line to ground faults. The fault location measured in fault case II by the distance relay in the R-X plane is shown in Figure 4.7.
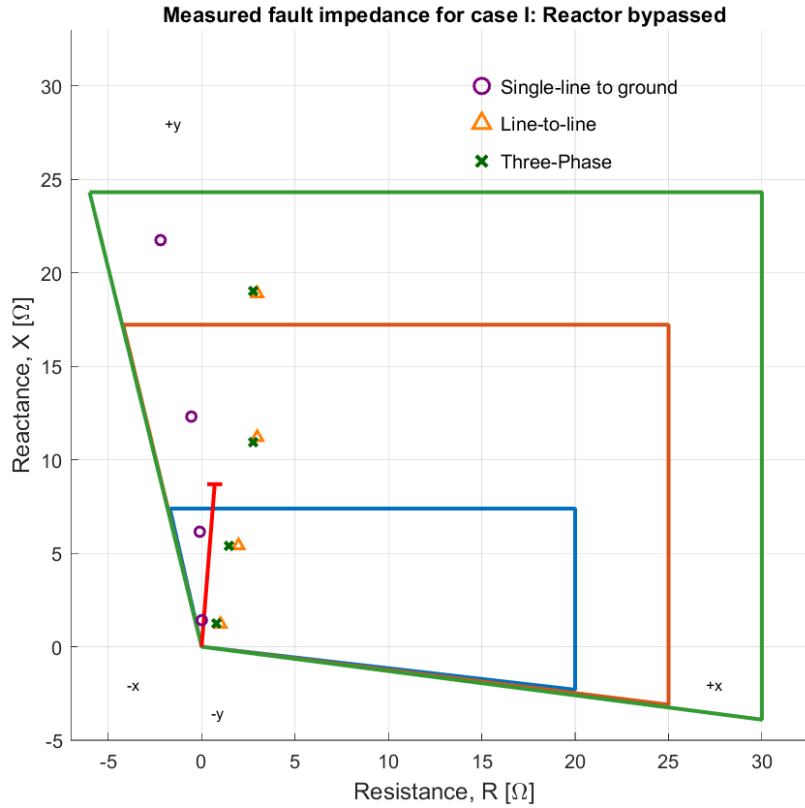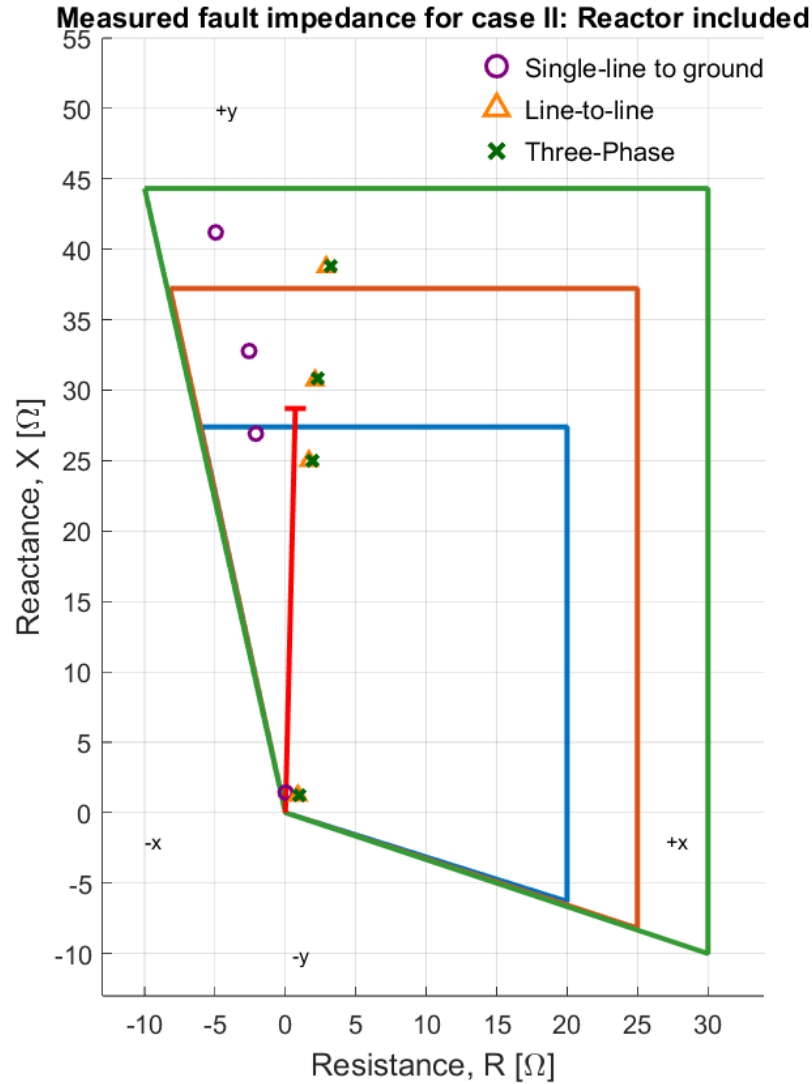

Figure 4.8: Fault impedance measured by the distance protection in PSCAD, where the series air-core reactor is included, Case II.

Figure 4.8 shows the data outlined in Table 4.2 for the measured impedance in case II

when the series air-core reactor is included. The overreaching in cases I and II for the single-line to ground fault implies that the distance protection function overestimates the actual fault location, which could potentially cause incorrect zone identification. The overestimation of the single-line to ground faults can be attributed to insufficient compensation for zero-sequence impedance and the effects of the mutual coupling of the parallel transmission lines. If the zero-sequence current is not accurately accounted for in the relay settings, it can lead to an overestimation of the apparent impedance seen by the distance relay. Additionally, mutual coupling between the parallel transmission lines induces voltages and currents due to magnetic coupling. These induced quantities may alter the voltage and current measured at the relay location, further distorting the impedance calculation.

The measured distance to the fault for the line-to-line and three-phase faults in both fault cases I and II is within acceptable limits, although slightly underestimating the distance to the fault. This observation is further supported by Figure 4.7 and Figure 4.8, which illustrate that the relay estimates the location of both fault types to be approximately the same location in the R-X plane.

To summarize, the distance relay, with the settings outlined in Section 3.6, has shown acceptable results as the distance relay has correctly detected and isolated all simulated fault types: single-line to ground, line-to-line, and three-phase faults. However, the single-line to ground faults have shown that the distance relay overestimates the distance to the fault between 5 % to 13 %, which raises concerns as this could potentially cause incorrect zone identification.

4.2.2 Simulation 2: Impact of the Fault Resistance

This section will analyze how the fault resistance affects the apparent impedance trajectory observed by the distance relay in the R-X plane. Thereby, evaluating the distance relays' ability to detect faults with various fault resistances. Figure 4.9 shows the apparent impedance trajectory for case I.2 for the single-line to ground fault with various fault impedances.

(a) Fault impedance of 0.01 ohm.

(b) Fault impedance of 0.1 ohm.

(c) Fault impedance of 1 ohm.

(d) Fault impedance of 5 ohm.
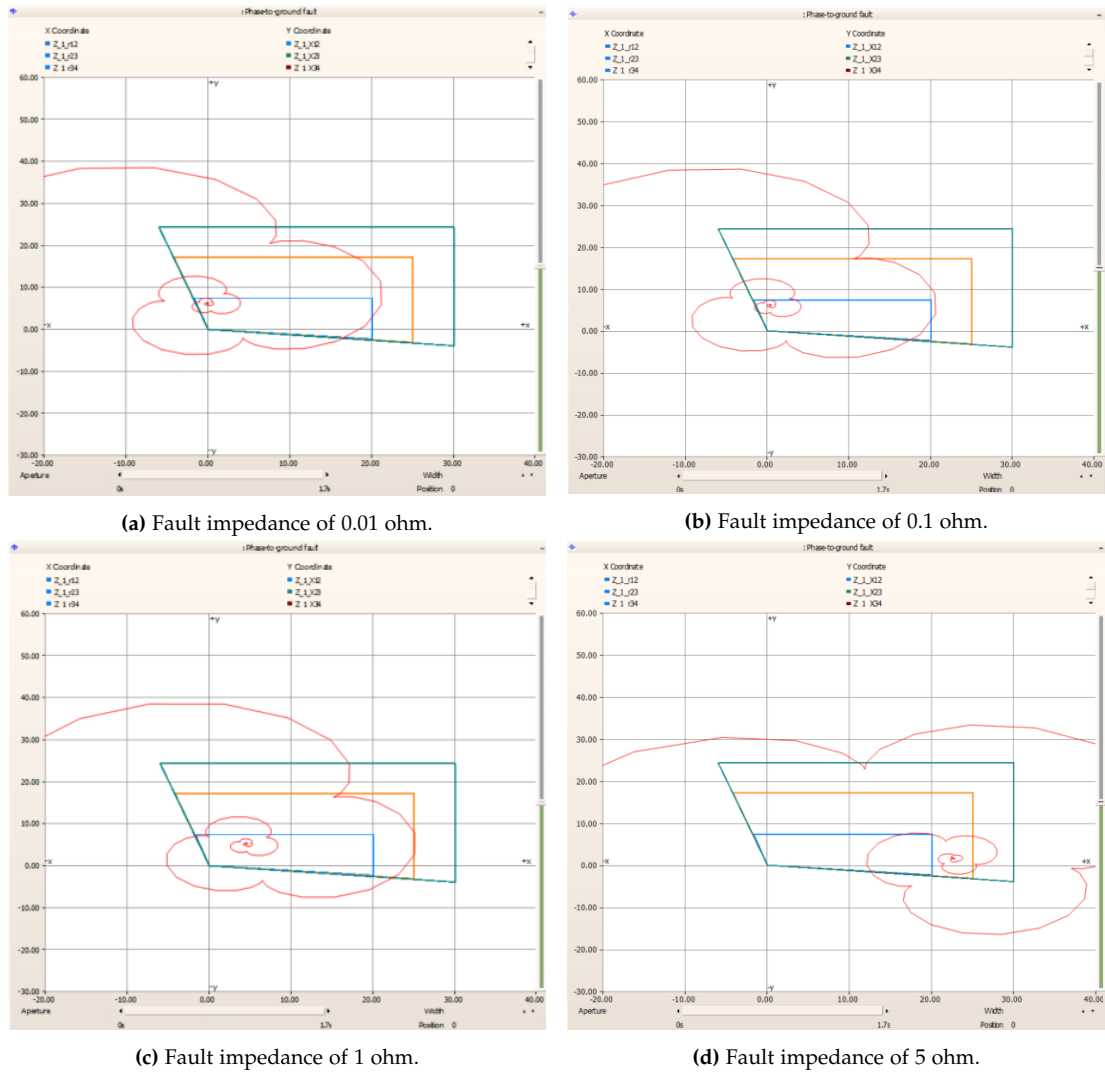
Figure 4.9: Effect of fault impedance on the apparent impedance trajectory for a phase-to-ground fault in case I, with the series air-core reactor bypassed.

Figure 4.10 shows the apparent impedance trajectories, with the series air-core reactor bypassed. With the four subfigures: 4.9a, 4.9b, 4.9c, and 4.9d, corresponding to fault resistances of $0.01\,\Omega$, $0.1\,\Omega$, $1\,\Omega$, and $5\,\Omega$, respectively.

Figure 4.9, shows a tendency that the impedance trajectory converges progressively more outwards on the resistive axis with the increasing fault impedance. In Figure 4.9d with a fault resistance of $5\,\Omega$, the fault is detected in zone 2, leading to misoperation of the distance relay. The impedance trajectory converges to a stable impedance measurement further outwards on the resistive axis than expected, which can be attributed to the influence of the in-feed from both sides on the fault. This phenomenon

also occurs in fault case II.2 when varying the fault impedance, which is shown in Figure 4.10.

(a) Fault impedance of 0.01 ohm.

(b) Fault impedance of 0.1 ohm.

(c) Fault impedance of 1 ohm.

(d) Fault impedance of 5 ohm.
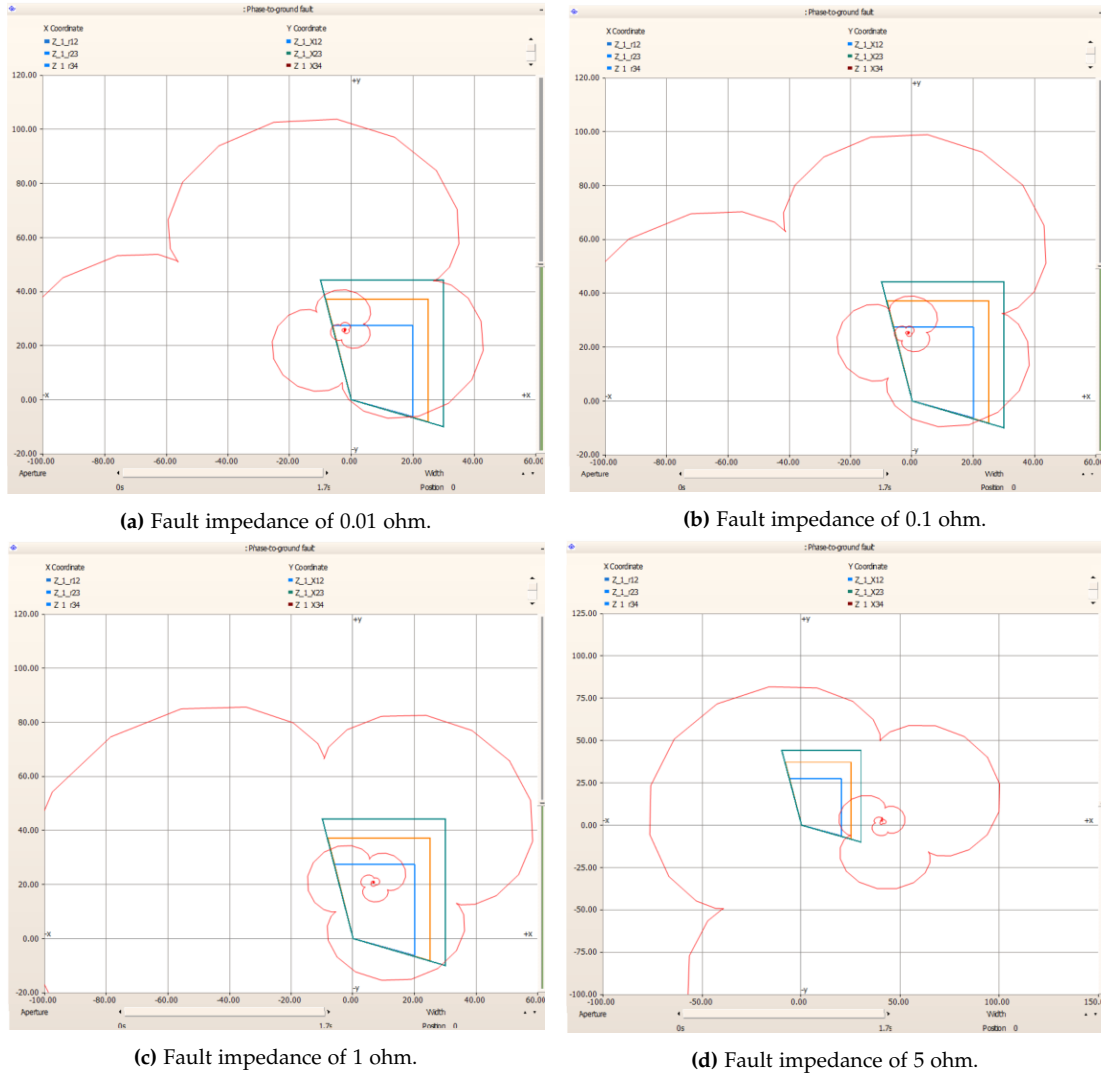
Figure 4.10: Effect of fault impedance on the apparent impedance trajectory for a phase-to-ground fault in case II, with the series air-core reactor included.

Figure 4.10 shows the apparent impedance trajectories, with the series air-core reactor included. With the four subfigures: 4.10a, 4.10b, 4.10c, and 4.10d, corresponding to fault resistances of $0.01\,\Omega$, $0.1\,\Omega$, $1\,\Omega$, and $5\,\Omega$, respectively.

The phenomenon shown in Figure 4.9 and Figure 4.10 with the increase in the measured fault resistance is attributed to the in-feed from both sides. In systems with in-feed from both terminals, the total fault current is the sum of the contributions

from the local end, I_1, and the remote end, I_2. However, the distance relay located at the local end measures the total voltage drop across the fault; however only measures the local end's contribution to the fault current. Thus leading to an overestimation of the impedance because the voltage drop across the fault resistance includes the total fault current (I_1+I_2), whereas the relay divides this voltage by only I_1. Therefore, the apparent impedance seen by the distance relay can be expressed in Equation (4.1). [15]

$$Z_{\text{App}} = \frac{V_{\text{A}}}{I_{\text{A}}} = \left(\frac{x}{l}\right) \cdot Z_{\text{L}} + R_{\text{F}} + \frac{I_2}{I_1} \cdot R_{\text{F}} \tag{4.1}$$

In Equation (4.1), Z_{L} is the total line impedance and $\frac{x}{l}$ is the fault location. The phenomenon leads to an apparent increase in fault resistance and consequently shifts the measured impedance further along the R-axis of the R-X plane. If not accounted for, it can lead to misoperation of the distance relay because the faults are not detected or detected in the wrong impedance zone. If there is no remote in-feed then $I_2 = 0$ and Equation (4.1) can be simplified by eliminating the term $I_2/I_1 \cdot R_{\text{F}}$. [15]

When comparing Figure 4.9d and Figure 4.10d, the measured impedance is further along the R-axis of the R-X plane when the series air-core reactor is included. This can be attributed to the series air-core reactor's impact on the transient current. The series air-core reactor lowers the transient current, thus the relation I_2/I_1 is higher, which means that the measured impedance is moved further along the R-axis of the R-X plane.

To summarize, the simulation has shown that the fault resistance impacts the distance relays' ability to detect faults. When the fault resistance is $1\,\Omega$ or lower, the distance relay is not significantly affected, and the fault remains within the desired impedance zone. However, when the fault resistance reaches $5\,\Omega$, it severely impairs the relay's detection ability, causing the fault to appear outside the intended impedance zone.

Chapter 5 Theoretical Calculations of Distance to the Fault

This chapter will calculate the theoretical distance to the fault based on the voltage and current measurements obtained in the PSCAD simulation. It will then investigate possible explanations for the discrepancies between the theoretically calculated and measured fault location in PSCAD.

5.1 Method of Calculating the Distance to the Fault

The distance protection relies on evaluating the apparent reactance between the relay location and the fault point. Hence, this section will outline the theoretical framework and equations utilize to estimate the distance to a fault based on the measured voltages and currents in PSCAD. The distance for the phase-to-phase faults is calculated using Equation (5.1), while the distance for phase-to-ground faults is calculated using Equation (5.2). [15] [41]

$$
\begin{aligned}
X_{\text{A-B}} = {} & \frac{V_{\text{A}} \cdot I_{\text{A}} \cdot sin(\varphi_{V_{\text{A}}} - \varphi_{I_{\text{A}}}) + V_{\text{B}} \cdot I_{\text{B}} \cdot sin(\varphi_{V_{\text{B}}} - \varphi_{I_{\text{B}}})}{I_{\text{A}}^2 - 2 \cdot I_{\text{A}} \cdot I_{\text{B}} \cdot cos(\varphi_{I_{\text{A}}} - \varphi_{I_{\text{B}}}) + I_{\text{B}}^2} \\[2mm]
& - \frac{V_{\text{A}} \cdot I_{\text{B}} \cdot sin(\varphi_{V_{\text{A}}} - \varphi_{I_{\text{B}}}) + V_{\text{B}} \cdot I_{\text{A}} \cdot sin(\varphi_{V_{\text{B}}} - \varphi_{I_{\text{A}}})}{I_{\text{A}}^2 - 2 \cdot I_{\text{A}} \cdot I_{\text{B}} \cdot cos(\varphi_{I_{\text{A}}} - \varphi_{I_{\text{B}}}) + I_{\text{B}}^2}
\end{aligned}
\tag{5.1}
$$

$$
X_{\text{Ph-E}} = \frac{V_{\text{Ph-E}}}{I_{\text{L}}} \cdot \frac{sin(\varphi_{V_{\text{Ph}}} - \varphi_{I_{\text{Ph}}}) - \frac{I_0}{I_{\text{L}}} \cdot \frac{R_{\text{E}}}{R_{\text{L}}} \cdot sin(\varphi_{V_{\text{Ph}}} - \varphi_{I_0})}{1 - \left(\frac{X_{\text{E}}}{X_{\text{L}}} + \frac{R_{\text{E}}}{R_{\text{L}}}\right) \cdot \frac{I_0}{I_{\text{L}}} \cdot cos(\varphi_{I_0} - \varphi_{I_{\text{L}}}) + \frac{R_{\text{E}}}{R_{\text{L}}} \cdot \frac{X_{\text{E}}}{X_{\text{L}}}(\frac{I_0}{I_{\text{L}}})^2}
\tag{5.2}
$$

However, Equation (5.2) does not account for the mutual coupling in the parallel lines, which can distort this impedance estimation. Equation (5.3) is utilized for the voltage as it represents the total voltage drop from the source to the fault, with compensation for the mutual coupling from the parallel line. [15] [41]

$$
V_{\text{Ph-E}} = I_{\text{L}} \cdot (R_{\text{L}} + jX_{\text{L}}) - I_0 \cdot \left(\frac{R_{\text{E}}}{R_{\text{L}}} R_{\text{L}} + j\frac{X_{\text{E}}}{X_{\text{L}}} X_{\text{L}}\right) - I_{\text{RM}} \cdot \left(\frac{R_{\text{M}}}{3R_{\text{L}}} R_{\text{L}} + j\frac{X_{\text{M}}}{3X_{\text{L}}} X_{\text{L}}\right)
\tag{5.3}
$$

By substituting Equation (5.3) into Equation (5.2), the resulting expression is given by Equation (5.4). [15] [41]

$$
X_{\text{Ph-E}} = \left|\frac{V_{\text{Ph-E}}}{I_{\text{L}}}\right| \cdot \frac{sin(\varphi_{V_{\text{Ph}}} - \varphi_{I_{\text{L}}}) - \frac{I_0}{I_{\text{L}}} \cdot \frac{R_{\text{E}}}{R_{\text{L}}} \cdot sin(\varphi_{V_{\text{Ph}}} - \varphi_{I_0}) - \frac{I_{\text{RM}}}{I_{\text{L}}} \cdot \frac{R_{\text{M}}}{3R_{\text{L}}} \cdot sin(\varphi_{V_{\text{Ph}}} - \varphi_{I_{\text{RM}}})}{1 - \left(\frac{X_{\text{E}}}{X_{\text{L}}} + \frac{R_{\text{E}}}{R_{\text{L}}} \cdot \frac{X_{\text{E}}}{X_{\text{L}}} \cdot \left(\frac{I_0}{I_{\text{L}}}\right)^2 + \frac{X_{\text{M}}}{3X_{\text{L}}} + \left(\frac{I_{\text{RM}}}{I_{\text{L}}}\right)^2 + \frac{R_{\text{M}}}{3R_{\text{L}}} \cdot \frac{X_{\text{M}}}{3X_{\text{L}}} \cdot \left(\frac{I_{\text{RM}}}{I_{\text{L}}}\right)^2\right)}
\tag{5.4}
$$

The variables utilized in Equation (5.1) through Equation (5.4) are defined as follows.

- V_A, V_B: Voltages in phases A and B, respectively.

- I_A, I_B: Currents in phases A and B, respectively.

- φ_{V_A}, φ_{V_B}: Phase angles of voltages in phases A and B.

- φ_{I_A}, φ_{I_B}: Phase angles of currents in phases A and B.

- $V_{Ph\text{-}E}$: Phase-to-earth voltage.

- I_L: Load or phase current.

- I_0: Zero-sequence current.

- I_{RM}: Zero-sequence current from the mutually coupled line.

- $\varphi_{V_{Ph}}$: Phase angle of the voltage during phase-to-earth fault.

- $\varphi_{I_{Ph}}$: Phase angle of the current during phase-to-earth fault.

- φ_{I_L}: Phase angle of the load current.

- φ_{I_0}: Phase angle of the zero-sequence current.

- $\varphi_{I_{RM}}$: Phase angle of the mutually coupled zero-sequence current.

- $\frac{R_E}{R_L}$, $\frac{X_E}{X_L}$, $\frac{R_M}{R_L}$, $\frac{X_M}{X_L}$: Line constant outlined in Chapter 3

The results of the calculated distance to the fault are outlined in Table 5.1.

Table 5.1: Example of a Sideways Table with a Caption

	Fault location impedance [Ω]	PSCAD impedance [Ω]	%Error	Theoretical impedance [Ω]	%Error
Bypass: Series air-core reactor					
Single-line to ground fault					
Case I.1	1.29	1.42	+10.56	1.29	+0.58
Case I.2	6.16	6.15	+9.17	6.20	+0.65
Case I.3	11.35	12.31	+8.86	11.51	+1.41
Case I.4	19.35	21.75	+12.74	19.53	+0.93
Line-to-line fault					
Case I.1	1.29	1.21	-5.84	1.28	-0.43
Case I.2	6.16	5.41	-3.96	6.14	-0.32
Case I.3	11.35	11.20	-1.51	11.33	-0.18
Case I.4	19.35	18.89	-2.55	19.33	-0.10
Three-phase fault					
Case I.1	1.29	1.26	-2.02	1.28	-0.38
Case I.2	6.16	5.38	-4.50	6.15	-0.16
Case I.3	11.35	10.96	-3.76	11.33	-0.17
Case I.4	19.35	19.02	-1.86	19.26	-0.47
Including: Series air-core reactor					
Single-line to ground fault					
Case II.1	1.29	1.43	+10.10	1.29	+0.62
Case II.2	25.40	26.91	+5.95	25.62	+0.86
Case II.3	30.90	32.78	+6.08	31.01	+0.36
Case II.4	38.91	41.20	+5.57	39.26	+0.91
Line-to-line fault					
Case II.1	1.29	1.22	-5.37	1.29	-0.51
Case II.2	25.40	24.98	-1.69	25.37	-0.14
Case II.3	30.90	30.70	-0.65	30.79	-0.35
Case II.4	38.91	38.75	-0.40	39.76	-0.37
Three-phase fault					
Case II.1	1.29	1.24	-3.67	1.29	-0.22
Case II.2	25.40	25.01	-1.57	25.35	-0.20
Case II.3	30.90	30.79	-0.35	30.80	-0.32
Case II.4	38.91	38.81	-0.24	38.78	-0.32

The theoretically calculated distance to the fault outlined in Table 5.1 is significantly more accurate than the measured distance in PSCAD for the single-line to ground faults. It should be noted that the theoretically calculated distance is still slightly more accurate in calculating the distance to the fault for phase-to-phase and three-phase faults.

The results in Table 5.1 show that when Equation (5.1) and Equation (5.4) are used to calculate the distance, the relay is more accurate. Thus, indicating that by utilizing an expression that more accurately accounts for zero-sequence impedance and mutual coupling effects between transmission lines, the distance relay can estimate the fault distance within acceptable limits for the single-line to ground fault.

The deviations between the actual distance and the theoretically calculated distance to the fault between the phase-to-phase and three-phase faults are improved across all test cases compared to the measured distance in PSCAD. The theoretically calculated distance uses more accurate equations, which are what is outlined in Siemens 7SA522 distance protection relay, which is a part of the Siprotec 4 series [41]. Thereby, Equation (5.1) and Equation (5.4) are expected to give a more realistic measurement of how a distance relay would calculate the distance to the fault.

It should be noted that there is a measuring error in PSCAD regarding the fault's exact location, which is less significant when the impedance is higher. This is not expected to have a significant impact on the results; however, it creates a possible error in the PSCAD measured impedance.

Chapter 6 Discussion

In this chapter, the various choices made throughout this project are discussed, including their impact on the results obtained in the PSCAD simulation and the following theoretical calculations. This involves the short-circuit contribution from the WTs and HVDC model, the deviations of results, and the limitations of the PSCAD model.

6.1 Short-circuit Contributions

Section 4.1 aims to verify the short-circuit current contributions for the models utilized in PSCAD as the WT type C, the WT type D, and the HVDC link. In Section 4.1, the short-circuit current contributions during single-line to ground, phase-to-phase, and three-phase faults are outlined with a fault resistance of 0.01 Ω.

When comparing the short-circuit contributions in Section 4.1 with what was expected based on Section 2.5 regarding the theoretical response of the WTs. Furthermore, the HVDC model provided short-circuit current contributions within acceptable limits of 1.2 p.u. to 1.7 p.u. of the nominal rated current, depending on the exact fault type. It should be noted that the HVDC model provided slightly more current for unbalanced faults compared to the current contributions of the balanced three-phase fault. The models utilized in this project are all PSCAD reference models, which have been slightly altered to fit the specifications. The PSCAD models for the HVDC link and WTs are considered to be accurate enough for the protection studies, which are performed in this project.

To summarize, the models have shown the expected results for the short-circuit current contributions. Thereby is the models are considered to provide accurate contributions for faults occurring with the fault impedance of 0.01 Ω.

6.2 Impact of the Series Air-core Reactor

Whenever the series air-core reactor is included in the simulations, the short-circuit current contributions are limited by adding inductive reactance. As any inductance introduced in a short-circuit current loop slightly decreases the rate-of-rise of short-circuit current. Furthermore, the addition of the 20 Ω series air-core reactors impacts the magnitude of the short-circuit current and voltage, which is described in Appendix C. This tendency does align with the expected short-circuit response, where the amplitude of the transient current is lower and the magnitude of the voltage breakdown is higher when the series air-core reactor is included. This indicates that simplifying the air-core reactor with a resistance and inductance provides acceptable results when evaluating based on the current and voltage waveforms.

The series air-core reactor impacts the transmission line impedance from Endrup to Revsing, which has led to the two different sets of impedance zone settings outlined

in Section 3.6. Having more than one set of impedance settings for distance relays is not uncommon for Energinet. Therefore, Energinet has allowed for the solution with two different impedance sets, dependent on the state of the air-core reactor.

The simulation results have shown that the distance relay, with the settings in Section 3.6 has correctly identified and isolated all test cases, including single-line to ground, phase-to-phase, and three-phase faults with and without the series air-core reactor correctly. Thus, the series air-core reactor does not affect the distance relay's ability to operate or its calculation of the distance to the fault, although it affects the short-circuit current and voltage waveforms.

6.3 CT Measuring Error

The results obtained in this project indicate that CT saturation is not a concern under the tested conditions. This is based on a comparison between the measured and calculated fault location using secondary-side measurements and the actual fault location set in the simulations. It should be noted that the CT measurements are from the weak end in-feed side in Endrup, thereby making it less likely that the CT would be affected.

6.4 Measuring Error in the PSCAD Simulation

When obtaining the fault impedance using PSCAD simulations, it was observed that the impedance trajectory in the R-X plane exhibits a small but noticeable fluctuation after the initial transient response. This means that the reactance value does not stabilize at a fixed point during the simulation time but continues to oscillate slightly around the expected impedance. The magnitude of this fluctuation is approximately $0.02\,\Omega$, even after the waveform appears to have settled. This introduces a measurement error, which is considered to be minor, that can affect the precision of the distance to the fault. This error becomes less critical for faults located further away from the distance relay and more prominent when the fault occurs nearby.

6.5 Deviation of the Measured and Calculated Distance to the Fault

The discrepancies between the measured and theoretically calculated fault distances can be attributed to the accuracy of the equations. In PSCAD, the distance protection is modelled as outlined in Section (3.6), using simplified equation blocks for both phase-to-phase and phase-to-ground faults, as shown in Figure 3.13a and Figure 3.13b, respectively. In modern distance relays such as the Siemens Siprotec 4 7SA522, both Equation (5.1) and Equation (5.4), presented in Section 5.1, are utilized

to calculate the distance to the fault. Notably, Equation (5.4) provides a significant improvement in accuracy for single line-to-ground faults, as it provides a more precise estimation of zero-sequence impedance and mutual coupling effects in transmission lines.

Therefore, is the lowered accuracy of the measured distance to the fault attributed to the limitations of the PSCAD software. AS when provided with the data from the simulations and compiling the distance to the fault in Equation (5.1) and Equation (5.4), it is possible to obtain more accurate results across all test cases when compared to the actual fault location.

6.6   Impact of the Fault Impedance

The impact of the fault impedance has been simulated in Section 4.2.2, which concluded that faults with in-feed from both sides are significantly impacted when the fault impedance reaches $5\,\Omega$. The phenomenon of in-feed from both terminals impacts the measurements as the total fault current is the sum of the contributions from the local end and the remote end. However, the distance relay located at the local end measures the total voltage drop across the fault, thus, it only measures the local end's contribution to the fault current. This leads to an overestimation of the impedance because the voltage drop across the fault resistance includes the total fault current. Yet the distance relay only accounts for the local current contributions. According to Equation (4.1), the fault resistance causes the measured impedance to shift further along the R-axis in the R-X plane. Thus, a larger fault resistance will impact the measured impedance more severely.

This has a negligible impact on the fault detection simulation in Section 4.2.1 and the theoretically calculated distance to the fault in Section 5.1. The impact is negligible as the fault impedance for all test cases is $0.01\,\Omega$, which also includes the data obtained to calculate the theoretical distance to the fault. As this project is focused on the distance relay in Endrup, which measures the weak in-feed characteristics from the WTs and HVDC model, would it be interesting to see the impacts that this has on the distance relay in Revsing, which measures the contributions for the grid side. It should be noted that if either of the distance relays notices a fault in zone 1, then it is allowed to remotely trip the relay other side of the fault. Whether this solves the problem with the in-feed from both sides is unknown. This should be further investigated, as this project does not cover the subject comprehensively enough to conclude on the impact that in-feed from both sides has on the distance relay in Revsing.

Chapter 7   Conclusion

In this Chapter, a conclusion of the project is presented. The manner in which the problem statement has been answered and the knowledge gained from this project will be assessed. This project set out to answer the following problem statement:

How can a suitable protection scheme be developed for the transmission line from Endrup to Revsing in a meshed transmission system, considering the integration of a series reactor, ensuring correct fault detection and relay operation?

An evaluation has been conducted on Energinet's standard protection scheme, comprising differential and distance relays, in a meshed transmission system with and without the presence of the air-core reactor. The air-core reactor is connected in series with a 400 kV parallel transmission line system interconnecting the substations of Endrup and Revsing. The theoretical framework detailed in Chapter 2 has concluded that the differential protection is unaffected by the series air-core reactor and parallel transmission line system, given that the CT provides accurate measurements. However, the distance protection is affected by the added impedance of the parallel transmission lines and the series air-core reactor. This project has proposed the solution of having two different impedance sets, with and without the series air-core reactor, to account for the added impedance.

Therefore, a PSCAD simulation was conducted to verify that the distance protection operates correctly in detecting and isolating faults, with both sets of impedance settings. The PSCAD simulation evaluates the distance protection under various test cases, including different fault locations, to verify the accuracy of the impedance zone settings. The results show that the distance relay overestimates the fault distance during single-line-to-ground faults with 8 % to 13 %, whereas it provides accurate estimates within acceptable limits for phase-to-phase and three-phase faults. The overestimation can be attributed to the current of the zero-sequence and mutual coupling between the parallel transmission lines, which has not been accurately accounted for. This is supported by the theoretical fault distance calculations, which yielded results with an error margin of less than 1 %. The theoretical calculation utilizes the voltage and current measurements from the PSCAD simulation to calculate the distance utilizing the equations as in the Siemens series 4 7SA522 distance relay.

To summarize, the overestimation of the distance to the fault for single-line to ground faults can be attributed to the limitation of the PSCAD software. As the equation utilized to calculate the distance to the fault is over-simplified, therefore not accurately account for the current contributions by the zero-sequence and mutual coupling. This can be solved by utilizing more accurate equations, which is the case for modern distance relays. Therefore, Energinet's standard protection scheme is considered to be adequate with the series air-core reactor if two impedance sets are utilized for the distance protection.

Chapter 8 Future Work

This chapter will outline some of the aspects which has not been adequately covered, yet still deemed interesting to investigate further. These aspects are concepts that could be improved, in the way some results were obtained, and also relevant concepts that were out of the scope of this project.

The series air-core reactors' impact on the differential protection has not been analyzed beyond the state-of-the-art outlined in Chapter 2. The theory strongly indicates that with accurate measurements of the CTs, the differential protection will be unaffected. However, the differential protection has not been tested in PSCAD. If tested, it would provide stronger evidence by verifying the entire protection system.

An interesting aspect that has not been covered is the impact of the mutual coupling of the parallel transmission lines. It would be interesting the see what the estimated distance to the fault would be in PSCAD if the parallel transmission line was disconnected. The simulation would aim to analyze the error that is caused in the simulation by the mutual coupling. This is expected to lower the error of the overestimation of the distance to the fault, while the would still be an error, which then mainly would be attributed to the zero-sequence current.

An extension to this project would be a study that involves testing the distance relay using PSCAD to generate a COMTRADE file, which captures the voltage and current waveforms. These files would be used to inject signals into a physical relay to evaluate its performance under transient replay conditions, thus verifying the responses to the transients in the simulation. This would provide a sense of security that the distance relay with the two sets of impedance settings would correctly detect and isolate faults, based on the provided data from the PSCAD simulation. Furthermore, can it be used to analyze the distance to the fault, which can be compared to the PSCAD measured, theoretically calculated, and actual induced distance to the fault to analyze whether the relays would need additional modifications regarding the zero-sequence or mutual coupling.

The distance protection in this proposed protection scheme would be considered to be back-up protection, as differential protection is considered to be faster in detecting faults. This project does not cover alternative protection methods to differential and distance protection. It would therefore be interesting to compare the performance to other methods, different from differential protection as over-voltage protection or under/over-frequency protection.

Bibliography

[1] Klima-, Energi- og Forsyningsministeriet, *Bekendtgørelse af lov om klima*, Dec. 2021. [Online]. Available: `https://www.retsinformation.dk/eli/lta/2021/2580` (visited on 02/06/2025).

[2] *Offshore wind farms tendered towards 2030 | Energistyrelsen*, en, Nov. 2024. [Online]. Available: `https://ens.dk/en/energy-sources/offshore-wind-farms-tendered-towards-2030` (visited on 02/06/2025).

[3] *Facts about solar energy | Energistyrelsen*, en, Nov. 2024. [Online]. Available: `https://ens.dk/en/energy-sources/facts-about-solar-energy` (visited on 02/06/2025).

[4] C. L. Bak and B. Bukh, *Energinet - Project Proposel*. [Online]. Available: `https://www.moodle.aau.dk/course/view.php?id=5298`.

[5] *High voltage series reactors for load flow control*, en-GB, 2004. [Online]. Available: `https://www.e-cigre.org/publications/detail/c2-206-2004-high-voltage-series-reactors-for-load-flow-control.html` (visited on 02/14/2025).

[6] S. M. Praminta, Y. Wicaksono, and H. Aji, "General Studies of Series Reactor and Phase Shifting Transformer in Java Bali Subsystem," in *2022 International Conference on Technology and Policy in Energy and Electric Power (ICT-PEP)*, Oct. 2022, pp. 123–127. DOI: `10.1109/ICT-PEP57242.2022.9988902`. [Online]. Available: `https://ieeexplore.ieee.org/document/9988902` (visited on 02/14/2025).

[7] A. S. Siddiqui, S. Khan, S. Ahsan, M. Khan, and Annamalai, "Application of phase shifting transformer in Indian Network," in *2012 International Conference on Green Technologies (ICGT)*, Dec. 2012, pp. 186–191. DOI: `10.1109/ICGT.2012.6477970`. [Online]. Available: `https://ieeexplore.ieee.org/document/6477970` (visited on 02/14/2025).

[8] "IEEE Guide for the Application of Protective Relaying for Phase-Shifting Transformers," *IEEE Std C37.245-2018*, pp. 1–71, May 2019, Conference Name: IEEE Std C37.245-2018. DOI: `10.1109/IEEESTD.2019.8721751`. [Online]. Available: `https://ieeexplore.ieee.org/document/8721751` (visited on 02/14/2025).

[9] M. Belivanis and K. R. W. Bell, "Use of phase-shifting transformers on the Transmission Network in Great Britain," in *45th International Universities Power Engineering Conference UPEC2010*, Aug. 2010, pp. 1–5. [Online]. Available: `https://ieeexplore.ieee.org/document/5649431` (visited on 02/14/2025).

[10] *Fault Current Limiter Using Series Reactors in Indian Power System*, en-GB, 2020. [Online]. Available: `https://www.e-cigre.org/publications/detail/c1-121-2020-fault-current-limiter-using-series-reactors-in-indian-power-system.html` (visited on 02/14/2025).

[11] *Phase shifting transformers installed in the Netherlands in order to increase available international transmission capacity*, en-GB, 2004. [Online]. Available: `https://www.e-cigre.org/publications/detail/c2-207-2004-phase-shifting-transformers-installed-in-the-netherlands-in-order-to-increase-available-international-transmission-capacity.html` (visited on 02/14/2025).

[12] M. Young, A. Dimitrovski, Z. Li, Y. Liu, and R. Patterson, "Continously variable series reactor: Impacts on distance protection using CCVTs," in *2015 IEEE Power & Energy Society General Meeting*, ISSN: 1932-5517, Jul. 2015, pp. 1–5. DOI: `10.1109/PESGM.2015.7286460`. [Online]. Available: `https://ieeexplore.ieee.org/document/7286460` (visited on 02/14/2025).

[13] *Energinet*, da, Feb. 2025. [Online]. Available: `https://energinet.dk/` (visited on 02/24/2025).

[14] *Overview | PSCAD*. [Online]. Available: `https://www.pscad.com/software/pscad/overview` (visited on 02/07/2025).

[15] G. Ziegler, *Numerical distance protection: principles and applications.* eng, 3. ed. Erlangen: Publicis Corporate Publishing, 2008, ISBN: 978-3-89578-318-0.

[16] *Guideline on the Impacts of Fault Current Limiting Devices on Protection System*, en-GB, 2008. [Online]. Available: `https://www.e-cigre.org/publications/detail/339-guideline-on-the-impacts-of-fault-current-limiting-devices-on-protection-system.html` (visited on 02/25/2025).

[17] G. Ziegler, *Numerical Differential Protection: Principles and Applications*, en. John Wiley & Sons, Jan. 2012, Google-Books-ID: sWLHKSN3pdUC, ISBN: 978-3-89578-670-9.

[18] O. S. E. Atwa, "Chapter 19 - Protection Relays Settings," in *Practical Power System and Protective Relays Commissioning*, O. S. E. Atwa, Ed., Academic Press, Jan. 2019, pp. 281–323, ISBN: 978-0-12-816858-5. DOI: `10.1016/B978-0-12-816858-5.00019-8`. [Online]. Available: `https://www.sciencedirect.com/science/article/pii/B9780128168585000198` (visited on 02/25/2025).

[19] *Impact of HVDC Stations on Protection of AC Systems*, en-GB, 2011. [Online]. Available: `https://www.e-cigre.org/publications/detail/484-impact-of-hvdc-stations-on-protection-of-ac-systems.html` (visited on 02/18/2025).

[20] *Fault current limiters in electrical medium and high voltage systems*, en-GB, 2003. [Online]. Available: `https://www.e-cigre.org/publications/detail/239-fault-current-limiters-in-electrical-medium-and-high-voltage-systems.html` (visited on 02/25/2025).

[21] T. N. Boutsika and S. A. Papathanassiou, "Short-circuit calculations in networks with distributed generation," *Electric Power Systems Research*, vol. 78, no. 7, pp. 1181–1191, Jul. 2008, ISSN: 0378-7796. DOI: `10.1016/j.epsr.2007.10.003`. [Online]. Available: `https://www.sciencedirect.com/science/article/pii/S0378779607002131` (visited on 02/26/2025).

[22] *Coordination of protection and automation for future networks,* en-GB, 2015. [Online]. Available: `https://www.e-cigre.org/publications/detail/629-coordination-of-protection-and-automation-for-future-networks.html` (visited on 03/04/2025).

[23] *Modern Distance Protection Functions and Applications*, en-GB, 2008. [Online]. Available: `https://www.e-cigre.org/publications/detail/359-modern-distance-protection-functions-and-applications.html` (visited on 03/05/2025).

[24] A. M. Tsimtsios and V. C. Nikolaidis, "Setting Zero-Sequence Compensation Factor in Distance Relays Protecting Distribution Systems," *IEEE Transactions on Power Delivery*, vol. 33, no. 3, pp. 1236–1246, Jun. 2018, Conference Name: IEEE Transactions on Power Delivery, ISSN: 1937-4208. DOI: `10.1109/TPWRD.2017.2762465`. [Online]. Available: `https://ieeexplore.ieee.org/document/8066310/?arnumber=8066310` (visited on 03/05/2025).

[25] F. Calero, "Mutual Impedance in Parallel Lines – Protective Relaying and Fault Location Considerations," en,

[26] J. G. Andrichak and G. E. Alexander, "Distance Relays Fundamentals," en,

[27] S. Anand, K. Kalita, and S. K. Parida, "A modified mutual impedance based backup protection for series-compensated transmission lines," *Electric Power Systems Research*, vol. 224, p. 109 719, Nov. 2023, ISSN: 0378-7796. DOI: `10.1016/j.epsr.2023.109719`. [Online]. Available: `https://www.sciencedirect.com/science/article/pii/S0378779623006089` (visited on 03/05/2025).

[28] *COBRAcable – Multi terminal HVDC-VSC link*, en. [Online]. Available: `https://vbn.aau.dk/en/projects/cobracable-multi-terminal-hvdc-vsc-link` (visited on 02/19/2025).

[29] W. Wang, M. Barnes, and O. Marjanovic, "The Impact of Control Design on Dynamic Behaviour of Multiterminal VSC-HVDC (MTDC) System under AC Grid Fault Conditions," English, in *IET Conference Proceedings*, Stevenage, United Kingdom: The Institution of Engineering & Technology, Apr. 2014, ISBN: 978-1-84919-815-8. DOI: `10.1049/cp.2014.0310`. [Online]. Available: `https://www.proquest.com/docview/1776444873/abstract/75AF01CF08A74722PQ/1` (visited on 03/18/2025).

[30] M. Ndreko, M. Popov, J. C. Boemer, and M. A. M. M. van der Meijden, "Sensitivity analysis on short-circuit current contribution from VSC-HVDC systems connecting far and large offshore wind power plants," in *IEEE PES Innovative Smart Grid Technologies, Europe*, ISSN: 2165-4824, Oct. 2014, pp. 1–6. DOI: 10.1109/ISGTEurope.2014.7028961. [Online]. Available: `https://ieeexplore.ieee.org/document/7028961` (visited on 03/18/2025).

[31] P. M. Anderson, *Power System Protection | IEEE eBooks | IEEE Xplore*, En, vol. 1999, ISBN: 978-0-470-54559-1. [Online]. Available: `https://ieeexplore.ieee.org/book/5264125` (visited on 03/06/2025).

[32] F. Blaabjerg, F. Iov, Z. Chen, and K. Ma, "Power electronics and controls for wind turbine systems," en, in *2010 IEEE International Energy Conference*, Manama, Bahrain: IEEE, Dec. 2010, pp. 333–344, ISBN: 978-1-4244-9378-4. DOI: 10.1109/ENERGYCON.2010.5771701. [Online]. Available: `http://ieeexplore.ieee.org/document/5771701/` (visited on 03/06/2025).

[33] E. Muljadi, N. Samaan, V. Gevorgian, J. Li, and S. Pasupulati, "Short circuit current contribution for different wind turbine generator types," in *IEEE PES General Meeting*, ISSN: 1944-9925, Jul. 2010, pp. 1–8. DOI: 10.1109/PES.2010.5589677. [Online]. Available: `https://ieeexplore.ieee.org/document/5589677` (visited on 03/06/2025).

[34] G. H. Li, B. H. Zhang, J. Wang, *et al.*, "Wind Farm Electromagnetic Dynamic Model and Outgoing Line Protection Relay RTDS Testing," in *2011 46th International Universities' Power Engineering Conference (UPEC)*, Sep. 2011, pp. 1–6. [Online]. Available: `https://ieeexplore.ieee.org/document/6125510` (visited on 03/06/2025).

[35] J. N. Nielsen, V. Akhmatov, J. Thisted, *et al.*, "Modelling and Fault-Ride-Trough Tests of Siemens Wind Power 3.6 MW Variable-Speed Wind Turbines," *Wind Engineering*, vol. 31, no. 6, pp. 441–452, Dec. 2007, Publisher: SAGE Publications, ISSN: 0309-524X. DOI: 10.1260/030952407784079753. [Online]. Available: `https://doi.org/10.1260/030952407784079753` (visited on 03/06/2025).

[36] V. Akhmatov, J. Nygaard Nielsen, K. Høj Jensen, *et al.*, "Siemens Wind Power Variable-Speed Full Scale Frequency Converter Wind Turbine Model for Balanced and Unbalanced Short-Circuit Faults," *Wind Engineering*, vol. 34, no. 2, pp. 139–156, Mar. 2010, Publisher: SAGE Publications, ISSN: 0309-524X. DOI: 10.1260/0309-524X.34.2.139. [Online]. Available: `https://doi.org/10.1260/0309-524X.34.2.139` (visited on 03/06/2025).

[37] R. P. Bataglioli, R. M. Monaro, and D. V. Coury, "Differential protection for stator ground faults in a full-converter wind turbine generator," *Electric Power Systems Research*, vol. 169, pp. 195–205, Apr. 2019, ISSN: 0378-7796. DOI: 10.

`1016/j.epsr.2018.12.018`. [Online]. Available: `https://www.sciencedirect.com/science/article/pii/S0378779618304152` (visited on 03/10/2025).

[38]   *HVDC VSC transmission interconnecting two AC systems*, en. [Online]. Available: `https://www.pscad.com/knowledge-base/article/222` (visited on 04/07/2025).

[39]   *COBRAcable*, en. [Online]. Available: `https://www.tennet.eu/projects/cobracable` (visited on 04/07/2025).

[40]   M. O Donovan, N. Barry, J. Connell, and E. Cowhey, "Mutual Coupling Compensation Techniques Used for Distance Protection of Parallel Lines," en, *Energies*, vol. 14, no. 7, p. 1982, Jan. 2021, Number: 7 Publisher: Multidisciplinary Digital Publishing Institute, ISSN: 1996-1073. DOI: `10.3390/en14071982`. [Online]. Available: `https://www.mdpi.com/1996-1073/14/7/1982` (visited on 04/14/2025).

[41]   *7SA522x_manual_a9_v047100_en.pdf - SIPROTEC 4 7SA522 Distance Protection - ID: 109743402 - Industry Support Siemens*. [Online]. Available: `https://support.industry.siemens.com/cs/document/109743402/siprotec-4-7sa522-distance-protection?dti=0&lc=en-DK` (visited on 05/19/2025).

Appendix A Distance protection: Secondary Side Impedance Settings

The impedance setting of the distance relay is converted to secondary side values of the instrument transformer; therefore is the VT and CT ratios are necessary to calculate the secondary side impedance. This is shown in Equation (A.2). [40]

$$Z_{\text{sec}} = \frac{V_{\text{sec}}}{V_{\text{prim}}} \cdot \frac{I_{\text{prim}}}{I_{\text{sec}}} \tag{A.1}$$

Equation (A.2) is used to calculate the ratio, Z_{sec}, from which the secondary side impedance can be obtained.

$$Z_{\text{sec}} = \frac{100\,\text{V}}{400\,\text{kV}} \cdot \frac{1.5\,\text{kA}}{1\,\text{A}} = 0.3750 \tag{A.2}$$

Impedance Setting: 1 Air-core Reactor Bypassed
The secondary side impedance of the instrument transformers is obtained by multiplying the setting values in Table 3.8 and the ratio calculated in Equation (A.2), and is outlined in Table A.1

Table A.1: The secondary side impedance setting for the distance relay at Endrup, where the air-core reactor is bypassed.

Grading (Reach)	$+R_{\text{reach,sec}}\,[\Omega]$	$+X_{\text{reach,sec}}\,[\Omega]$	Time delay [s]
Zone 1	0.2230	2.7717	0.0
Zone 2	0.3920	6.4590	0.3
Zone 3	0.5534	9.1186	0.8

Impedance Setting: 2 Air-core Reactor Included
Similarly, when the impedance setting with the series air-core reactor is bypassed, the secondary impedance settings are calculated using Table 3.9 and Equation (A.2), giving the results outlined in Table A.2.

Table A.2: The secondary side impedance setting for the distance relay at Endrup, where the air-core reactor is included.

Grading (Reach)	$+R_{\text{reach,sec}}\,[\Omega]$	$+X_{\text{reach,sec}}\,[\Omega]$	Time delay [s]
Zone 1	0.2267	9.1459	0.0
Zone 2	0.3957	13.4841	0.3
Zone 3	0.5571	18.1180	0.8

Appendix B Measuring Data Utilized to Calculate the Distance to the Fault

This Chapter will detail how the distance to the fault is computed in the simulation and calculation. To compute the distance to the fault, the short-circuit current and voltage values must be stored. The window of data during a fault that is necessary to store is outlined in Figure B.1
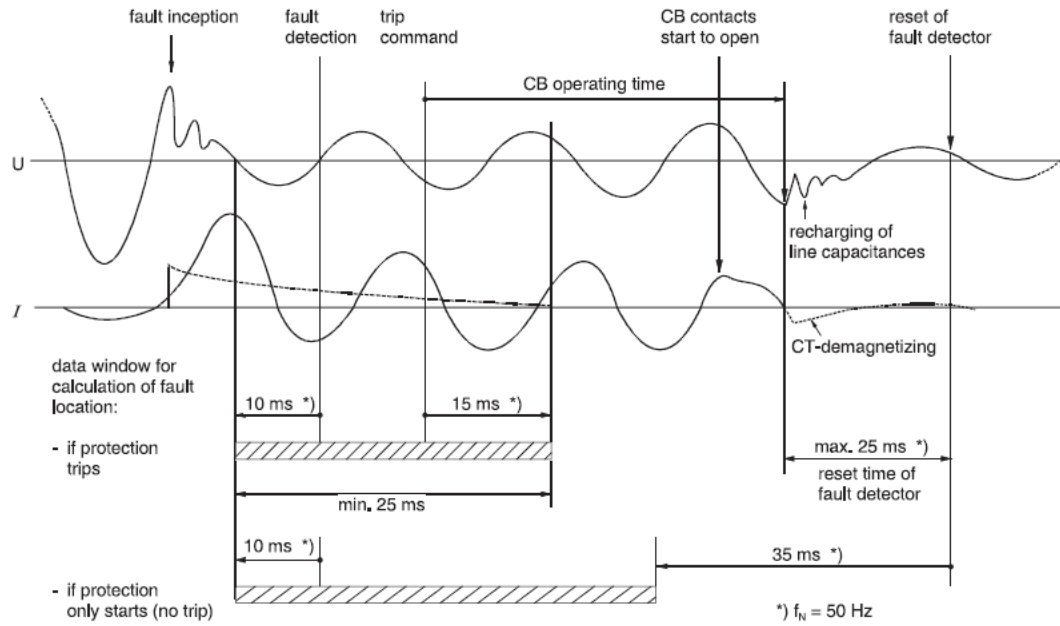

Figure B.1: The data window for the distance fault computation. [15]

Figure B.1 shows that the calculation of the fault distance is performed using the recorded short-circuit current and voltage measurements. This measurement window is placed immediately after fault inception and concludes before the operation of the circuit breaker. It should be noted that the comparison between the measured distance to the fault in PSCAD and the theoretically calculated distance to the fault is completed using the same time stamp. The same time stamp is utilized for comparison, which means that the error can be attributed to the impedance measurement in the PSCAD RX-plane.

Appendix C Mutual Coupling of the Transmission Line in PSCAD

This Chapter will outline the difference in the current and voltage waveforms when bypassing and including the series air-core reactor. This aims to verify that the simplification of the series air-core reactor provides the expected impact of the current and voltage waveforms. The current and voltage waveforms, while the series air-core reactor is bypassed, during a single-line to ground fault are shown in Figure C.1.
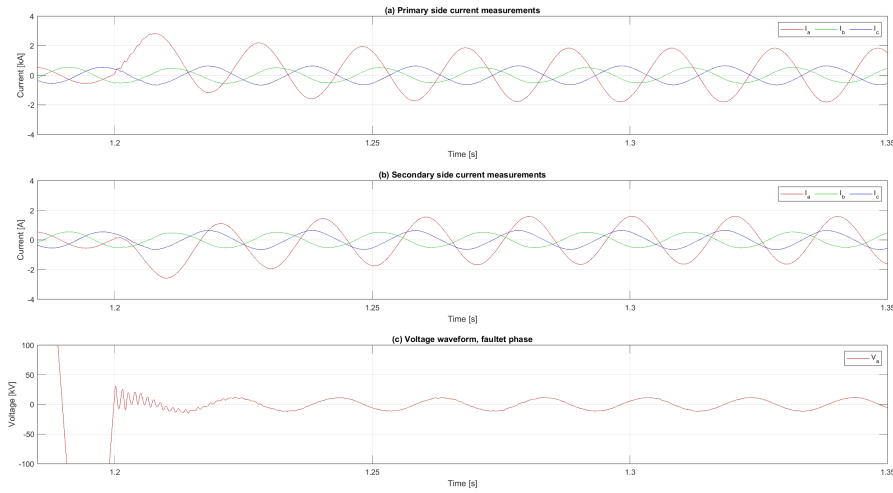

Figure C.1: Current and voltage measurements bypassing the series air-core reactor.

Figure C.1 shows an initial current peak in the faulted phase, which is measured in both the primary side and secondary side of the CT. Furthermore, Figure C.1 shows that the voltage collapsed post-fault. Figure C.2 shows the current and voltage waveforms when the series air-core reactor is included.
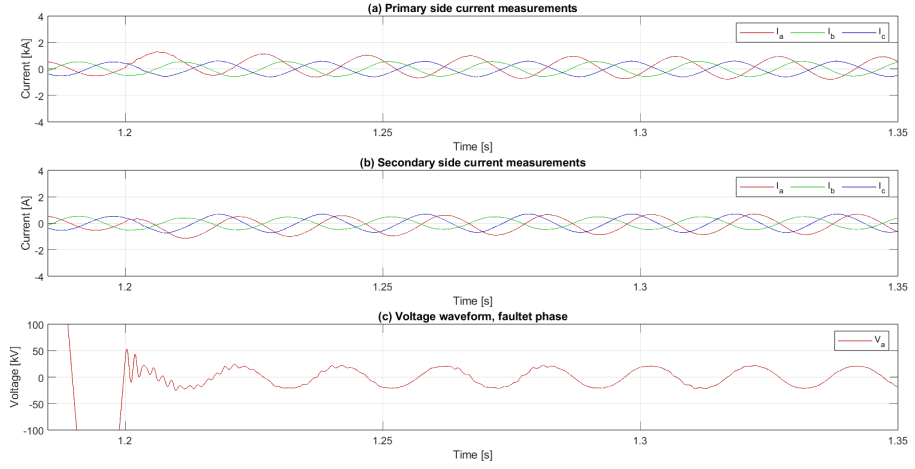
Figure C.2: Current and voltage measurements including the series air-core reactor.

When comparing the waveforms when the series air-core reactor is bypassed and included in Figure C.1 and Figure C.2, respectively. When the series air-core reactor is included, the transient current magnitude decreases, and the voltage drop is slightly mitigated. These effects are as expected since the reactor limits the fault currents and supports the voltage stability.

The results in Figure C.1 and Figure C.2 are from a test case where the contributions of the WTs and HVDC link are halved. By halving the contributions, the study assesses the impact of diminished source influence on the protection system's performance, providing insights into the relay's sensitivity under varying generation conditions.